journal of the international meteor organization

WGN

50:2
april 2022

Jupiter family meteor showers explored in SonotaCo data
Role of meteoric influx and geomagnetic disturbance on sporadic E
Third Quarter 2019 IMO video meteors

ISSN 1016-3115

WGN Vol. 50, No. 2, April 2022, pp. 35 – 70

Administrative

Meteor Science

Preliminary results

Front cover photo

Impressive fireball photographed a little ways down the coast Lulworth Cove, England, on 2022 April 9, at $02^{h}41^{m}$ UT. For more information, photos, and videos on this fireball, visit the event page at `https://fireball.imo.net/members/imo_view/event/2022/2147`. Photo courtesy: Alison Fairley.

Writing for WGN

This Journal welcomes papers submitted for publication. All papers are reviewed for scientific content, and edited for English and style. Instructions for authors can be found in WGN **45:1**, 1–5, and at `http://www.imo.net/docs/writingforwgn.pdf` .

Legal address

International Meteor Organization, Jozef Mattheessensstraat 60, 2540 Hove, Belgium.

Editorial — Call for papers

Javor Kac

The Tau Herculids served us the long-awaited outburst at the end of 2022 May.

Having observed the Tau Herculids outburst from Arizona in the US, I was thrilled to see meteors from this until now hardly observable meteor shower. I know many meteor enthusiasts in the Americas and those flying from overseas have also enjoyed the outburst in good conditions, while others settled for more close-by or home locations to observe the shower.

I am therefore inviting individuals and groups to submit articles about your Tau Herculids observations. These could range from descriptions of your observational location and campaign and observing setup, to your preliminary or intermediate results.

Other kinds of meteor-related articles are of course also welcome.

For instructions for authors, please see `https://www.imo.net/publications/wgn/` or Kac (2017).

References

Kac J. (2017). "Writing for WGN". *WGN, Journal of the International Meteor Organization*, **45:1**, 1–5.

IMO bibcode WGN-502-editorial NASA-ADS bibcode 2022JIMO...50...35K

IMO Meteor Shower Calendar for 2023

Jürgen Rendtel[1]

This annual IMO publication was initiated and edited over many years by Alastair McBeath, and it now sees its thirty-third edition. One main goal is to draw the attention of observers to both regularly returning meteor showers and to events which may occur according to model calculations. The other goal is to spread the information early enough for inclusion into other compilations. The latter goal also determines the publication date in the middle of the year while the observers perhaps might wish to have later results from returns being considered.

For the annual showers, we use the data collected by visual, video and radion forward scatter observations over the previous years. Additionally, I had information about possible meteor activty from various publications such as Peter Jenniskens' book on meteor showers and their parent objects, Mikhail Maslov's web pages with personal comments from him. Jérémie Vaubaillon provided me with a compilation of modelling results concerning known streams as well as possible encounters with dust from various objects which may cause detectable meteor activity. Among these is a first approach of the Earth to dust ejected from comet 46P/Wirtanen in December.

Within a small working group in the IMO we discussed the entries in the working list of meteor showers. I am particularly thankful to Masahiro Koseki who added important data and comments about several showers which required modifications in the list. For example, the maximum of the Southern Taurids is given now to occur in early November according to observational data. The previously given October date coincides with another but smaller increase of the ZHR of this complex shower. We newly introduced the η-Eridanids in August as this shower is regularly found in several data. The daytime showers, observable essentially with radio techniques only, needs to undergo a revision for the next calendar. For the 2023 edition we updated the data as far as possible now, considering more recent information.

The working list always needs input from observers to confirm or adjust the provided information. So the publication of the calendar is meant as a bi-directional exchange. Each data set may help to improve the basis for the understanding of the meteoroid streams and to provide reliable data for the upcoming editions.

Last but not least thanks to Tim Cooper, Robert Lunsford, Alastair McBeath, Ina Rendtel and Chris Steyaert for carefully checking the contents. The calendar is available from the IMO web page and will also be mailed with the next (printed) WGN issue. Please feel free to distribute the calendar so that the available information is spread and we may encourage observers worldwide to collect and submit data which can be used for meteor shower studies.

[1] International Meteor Organization, Eschenweg 16, 14476 Potsdam, Germany. Email: `jrendtel@web.de`

Meteor Observer Handbook – new edition 2022

Jürgen Rendtel[1]

The 2022 edition of the IMO's *Meteor Observer Handbook* is now available! Here are some accompanying remarks from the point of view of the Editor.

The IMO's first version of an Observer Handbook published in 1995 was primarily written for visual meteor observers and included a section of meteor shower descriptions. It was a compilation of several contributions by more than a dozen authors. The next (2008) edition included descriptions of other observing techniques as well as a brief section about data analysis, deriving parameters such as the population index or spatial number densities. We also found that the shower secriptions are of course useful, but almost each return of a shower brought new results which were not reflected in the book. Remember that between 1995 and 2008 we experienced a series of strong Perseid peaks and Leonid outbursts, connected with a rapid increase of our knowledge about meteoroid streams and their evolution. The list of peculiar events in that period is quite long and includes the return of the June-Bootids (1998), the predicted and well-observed α-Monocerotid (1995) and Aurigid (2007) outbursts. Therefore we separated the Shower Chapter from the descriptions of the observing and analysing methods when the 2013 edition of the Handbook was prepared. (An update of the Shower Workbook, last published in 2014, is on its way.)

The evolution of observing techniques imply both additions to some sections while others become obsolete. For example, the former field of telescopic observations is completely covered by video cameras now and meteor photography changed from providing data for calculations of atmospheric meteor trajectories and meteoroid orbits to producing aesthetic images, with the exception of meteor spectra. In this context, it seems surprising that visual observations still play an important role for shower studies – such observations allow us to combine historic and recent shower data to establish a long-term data base. They are also helpful to calibrate modern video data.

The 2022 edition is again a compilation of contributions. The chapters have been revised, extended or newly written. As the Editor, I am happy that so many authors – given for each chapter – and others who remain behind the scenery helped and contributed to the book. Many of these helpers are at least listed in the acknowledgements. The introducting chapter has some of the background for understanding the various phenomena including fireballs and meteorite falls. The currently existing camera networks, their aims and technical background are given in the video observations chapter. Large portions of the text about photography has been kept, but information about spectra and unusual meteor trails are added. Apart from the technical details of forward scatter meteor observations, the chapter now also has information about shower data derived from the raw data. The analysis chapter got the largest extension, including a complete description and evaluation of the steps from raw data to physical parameters of meteoroid streams and their accuracy. Since we often state that we have to apply statistical methods, this chapter now also has a section about a stochastic treatment of meteor shower data. I am also grateful for Peter Brown's Foreword which describes the contents from another perspective. Last but not least, we updated the extended Glossary which may serve as a reference by itself.

At the end it took more time than initially planned to have this edition published. I hope the result was worth waiting and wish all observers clear skies and fascinating meteor events. The printed book is available from the IMO web shop; IMO members may access the PDF via their account on the web page.

Publication details:

Handbook for Meteor Observers, IMO 2022
Editor: Jürgen Rendtel
180 pages, ISBN 978-2-87355-034-9
Chapter 1: Meteor astronomy (Jürgen Rendtel)
Chapter 2: Visual meteor observations (Jürgen Rendtel, Rainer Arlt, Ralf Koschack)
Chapter 3: Visual observations of minor showers (Rainer Arlt, Jürgen Rendtel, Ralf Koschack)
Chapter 4: Video observations (Sirko Molau, Pete Gural)
Chapter 5: Photographic observations (Jürgen Rendtel, William Ward)
Chapter 6: Radio meteor observations (Cis Verbeeck, Jean-Louis Rault)
Chapter 7: Analyses and calculations (Ralf Koschack, Jürgen Rendtel, Janko Richter)

[1] International Meteor Organization, Eschenweg 16, 14476 Potsdam, Germany. Email: jrendtel@web.de

International Meteor Organization

HANDBOOK FOR METEOR OBSERVERS

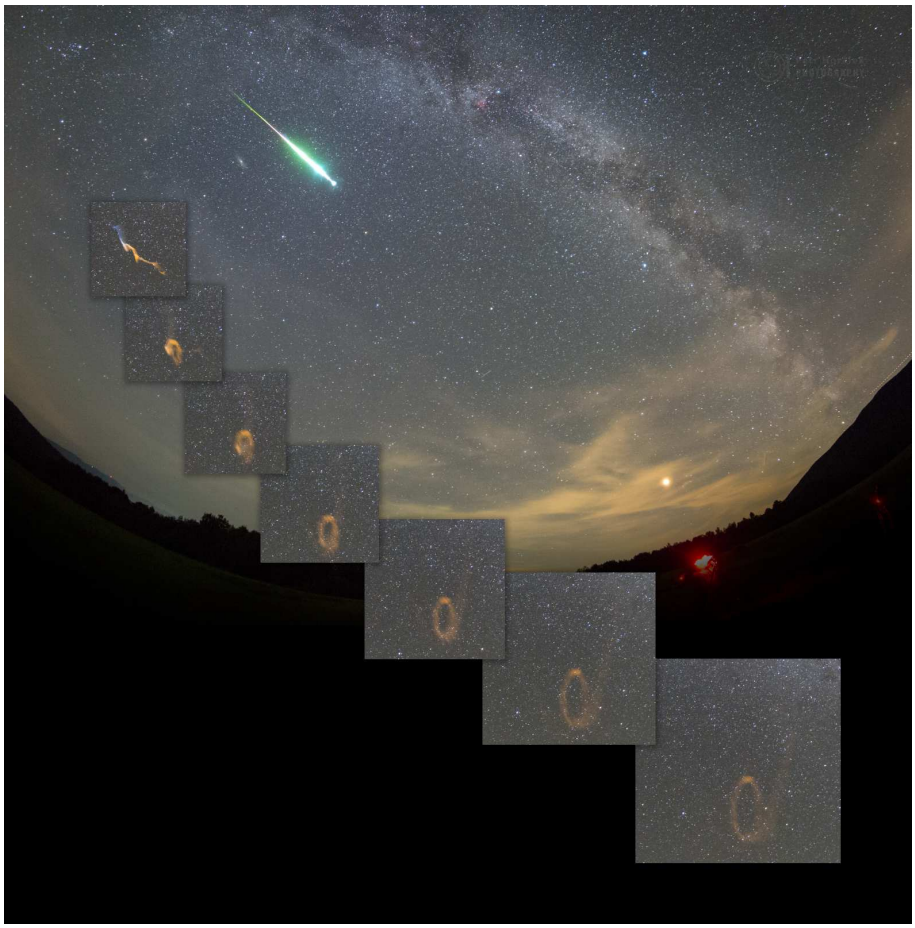

Edited by
Jürgen Rendtel
2022

Figure 1 – IMO's *Meteor Observer Handbook* front cover. The cover image shows a Perseid fireball which appeared on 2018 August 12, 21:55:07.67 UTC over Kolonica Observatory, Czech Republic – Petr Holácek.

Meteor Science

Jupiter Family Meteor Showers by SonotaCo Network Observations

Shiba, Yasuo [1]

I investigated Jupiter family meteor showers using fourteen years of records, 2007 till 2020, from the database of the Japanese automatic TV meteor observation network, the "SonotaCo network". Out of the results, 38 meteor showers have been published as "established meteor showers" at the IAU Meteor Data Center, 17 meteor showers were on the IAU MDC working list and 1 new meteor shower's elements were found. Comparing this study and the IAU MDC, I propose two improvements for the IAU MDC registration process: (1) To register meteor showers at the IAU MDC by checking four requirements involving scientific data, the shower's existence, the shower's independence from already known showers, and the research's objectivity; and (2) In the shower's "Activity" classification, adding a new division "periodic" or "resonance" to the current categories of "annual" and individual years.

Received 2022 February 19

1 Introduction

The "SonotaCo network" (SonotaCo, 2009) is a Japanese automatic TV meteor observation network whose results starting from 2007 have produced great progress in meteor investigations. The SonotaCo network's high performance and user-friendly observation tools contribute not only to Japanese amateur meteor observers but observers worldwide who have presented many papers. The accumulation of stable data from 2007 till 2020 is over an orbital period of Jupiter and so we can research mean motion resonance phenomena with Jupiter. I tried to find out in this paper the Jupiter family meteor shower activity variation characteristics for every year.

2 Methods

The studied meteor orbits are calculated by using UFOOrbit V2 based on download data from the SonotaCo Network site (SonotaCo, 2009) which were uploaded by individual network observers. The research period is from 2007 January till 2020 December. Observers' TV cameras recorded meteors concentrated specifically over the sky region of central Japan. The total number of calculated meteor orbit data is 298 689. Meteor numbers for 10° solar longitude bins are shown in Figure 1(a) and for every year in Figure 1(b). The curve superposed on Figure 1(a) is the approximate observable time over one night. The decrements in meteor numbers relative to observable time around 90° and 180° solar longitude are rainy seasons in Japan. Figure 1(b) indicates meteor number variations are not too large from year to year. It suggests the data are enough that we can research meteor shower activity varying over years.

UFOOrbit V2 calculation results contain a few meteor initial velocity errors that are generated by the mean calculation method from only the beginning and end points. But the meteor velocity is decelerated by the Earth's atmosphere. This effect makes it possible to underestimate the velocity for individual meteors. Generally, if a meteor path is through to a low atmospheric height where there is a high air density environment, then atmospheric deceleration is increased. This corresponds to slow initial velocity and heavy initial mass meteoroids. The underestimate can be corrected in UFOOrbit V2 with the value "V_{io}" which is the meteor initial velocity correction value. Thus, I estimated V_{io} from a few meteor showers where mean motion resonances exist with Jupiter's orbital period. These meteor

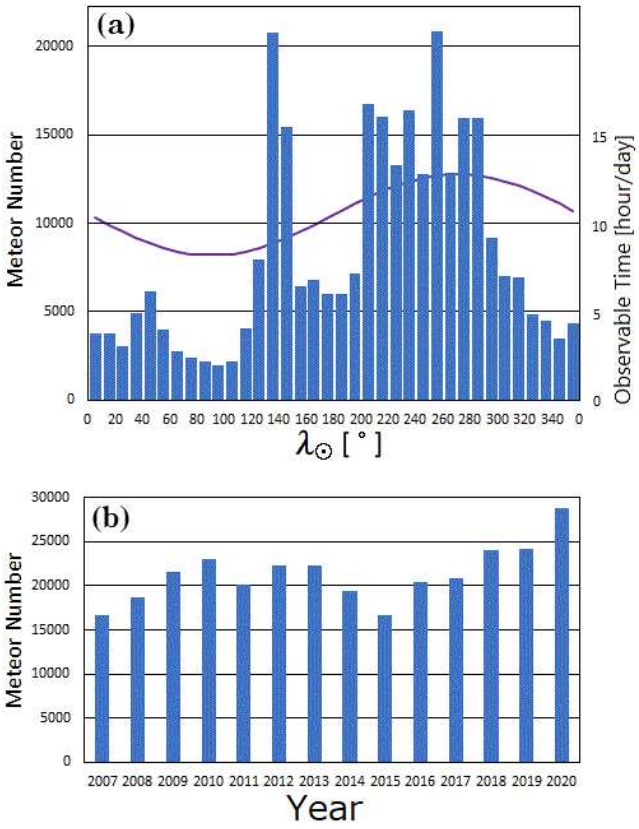

Figure 1 – SonotaCo meteor numbers as a function of (a) solar longitude and (b) year.

[1](SonotaCo network)
673-0882, Aioi town 2-18-7-404, Akashi-city, Hyogo prefecture, Japan.
Email: kqc43540@biglobe.ne.jp

IMO bibcode WGN-502-shiba-jupiter
NASA-ADS bibcode 2022JIMO...50...38S

Table 1 – "V_{io}" value (deceleration by the atmosphere) estimation.

	Shower	V_{io} [km/s]
Jupiter Family	STA	0.97
	EVI	0.63
	KCG	0.68
Halley Type	PER	0.25
	LEO	0.22
	ORI	0.4
	ETA	0.28

showers' accurate orbital period can be decided easily, and as a result an accurate semi major axis determined. Estimated V_{io} are shown in Table 1 for three Jupiter family meteor showers with such resonances. Additionally, Halley type meteor showers' V_{io} estimated from the parent body period are shown in the lower part of Table 1. Table 1 indicates slower velocity Jupiter family meteor showers require a larger V_{io} value than faster Halley type meteor showers. EVI and KCG require a similar V_{io} but STA is the largest V_{io}. The reason is thought to be caused by the STA annual component that is active simultaneously with the resonance component of STA (Shiba, 2016). The non-resonance annual component STA mean orbital period is smaller than the period of the resonance component during the season when both components are active. Contamination from the STA annual component can induce the requirement for a larger V_{io}. I adopted the V_{io} value based on EVI and KCG but not the STA value. EVI and KCG include many numbers of larger meteoroid particles and lower atmospheric end height meteors compared with many Jupiter family meteor showers. As a result, I took a V_{io} value of 0.5 km/s.

Investigated meteor showers were selected from those at the IAU Meteor Data Center (Jopek & Jenniskens, 2011; Jopek & Kaňuchova, 2014, 2017; Jenniskens et al., 2020; Neslušan et al., 2020) described as "established meteor showers" in 2021 July, by considering the following conditions: (1) The orbital period is shorter than Jupiter's; (2) The meteor orbit comes closer to Jupiter's orbit than 2.5 AU; (3) The meteor radiant exists at an observable declination from Japanese latitudes (about +35°); and (4) The radiant position is far enough from the Sun to observe by optical techniques. The total number of selected meteor showers is 41. I researched additionally established meteor showers' border area for radiant position and duration. I also researched the antihelion region radiant map that includes many Jupiter family meteor showers. These additional meteor showers were 17 on the IAU MDC working list and 1 new meteor shower. However, #183 PAU, #187 PCA, #319 JLE, #530 ECV, #569 OHY (IAU MDC numbers and codes) were determined as Halley type meteor showers and removed from this study. #320 OSE and #15 URS were concluded as Halley type but their results are included in this study because they are related to the Jupiter family meteor showers considered.

Methods to decide meteor shower membership are as follows. Figures were plotted using the two types of coordinates below, and then meteors in regions of radiant concentrations were taken as shower members but meteors in other regions were removed.

(1) Radiant position ($\alpha : \delta$) or ($\lambda - \lambda_\odot : \beta$)

(2) ($\lambda_\odot : V_g$)

where α = right ascension, δ = declination, $\lambda_\odot$ = solar longitude, λ = ecliptic longitude, β = ecliptic latitude and V_g = geocentric velocity.

Next, the D criterion (D_d) was calculated for individual meteors (Drummond, 1981) compared with the selected meteor mean orbit. I excluded $D_d > 0.105$ meteor orbits as not similar. For long term continuous active meteor showers the above treatment was applied for each 10° bin in solar longitude and if a continuous area of concentrated radiants existed, decided as one independent meteor shower.

3 Results

3.1 Data catalogue of meteor showers

Calculated results are shown in Table 2. Columns from left are

Est.: Established meteor shower or not,
No.: IAU MDC shower number,
Meteor Shower Name: IAU MDC shower name,
Code: IAU MDC code number,
Activity: Form of activity or active years,
$\lambda_\odot$: Mean solar longitude,
$\lambda_\odot$ beg: Solar longitude at beginning of activity,
$\lambda_\odot$ end: Solar longitude at end of activity,
α: Corrected radiant point mean right ascension,
δ: Corrected radiant point mean declination,
dα: Radiant drift of α for 1° solar longitude,
dδ: Radiant drift of δ for 1° solar longitude,
V_g: Mean geocentric velocity,
dV_g: Variation in V_g for 1° solar longitude,
R.P.±: Radiant distribution radius,
V_g±: Geocentric velocity dispersion,
a: Semi major axis,
q: Perihelion distance,
e: Eccentricity,
P: Orbital period,
Peri: Perihelion argument,
Node: Ascending node longitude,
Incl: Inclination,
N: Recorded number of meteors,
mag: Mean absolute magnitude,
γ: Luminous index,
H_1: Beginning luminous height above sea level,
H_2: Ending luminous height above sea level.

3.2 Individual meteor showers

3.2.1 alpha Capricornids (#001 CAP) and xi2 Capricornids (#623 XCS)

Activity features vary for individual years and detailed evaluation could not be easy because it includes the rainy season. As to the detail, 2012 and 2016 sky conditions were estimated as the same sky level, however, the 2016 radiant distribution was more sparse than

Table 2 – Individual meteor shower results. Explanation of column headings is given in Section 3.1.

Est.	No.	Meteor Shower Name	Code	Activity	$\lambda_\odot$	$\lambda_\odot$ beg	$\lambda_\odot$ end	α	δ	dα	dδ	V_g	dV_g	R.P.±	V_g±	a	q	e	P	Peri	Node	Incl	N	mag	γ	H_1	H_2
								[deg] J2000				[km/s]		[deg]	[km/s]	[AU]	[AU]		[yr]	[deg] J2000				[mag]		[km]	[km]
O	1	alpha Capricornids	CAP	annual	115.2	105	120	300.0	−11.9	0.63	0.24	25.0	−0.17	3	2.5	2.400	0.496	0.793	3.72	279.1	115.2	7.6	142	−0.75	1.6	94.7	83.5
					124.1	120	127	304.3	−9.9	0.49	0.25	23.2	−0.25	2.5	2	2.586	0.569	0.780	4.16	270.2	124.1	7.5	280	−1.20	1.7	94.1	81.7
					130.4	127	138	307.7	−8.3	0.54	0.28	21.9	−0.19	2.5	2	2.584	0.613	0.763	4.15	265.2	130.4	7.4	466	−1.30	1.4	93.6	81.4
O	2	Southern Taurids	STA	periodic	224.5	210	240	54.9	14.6	0.55	0.05	28.0	−0.29	2	1.5	2.122	0.367	0.827	3.09	113.1	44.5	5.4	1027	−1.11	2.0	96.4	74.1
			STA	annual	202.4	187	213	36.8	9.7	0.80	0.25	28.6	−0.05	5	4	1.813	0.311	0.828	2.44	121.3	22.4	5.7	1050	0.14	3.3	95.9	79.5
					221.6	213	231	51.8	13.7	0.70	0.13	27.4	−0.15	5	3.5	2.034	0.374	0.816	2.90	112.7	41.6	5.4	1212	−0.20	3.1	95.4	77.8
					242.1	231	258	65.3	14.9	0.69	0.01	23.4	−0.17	5	3.5	2.105	0.515	0.756	3.05	96.4	62.1	5.2	958	−0.32	2.1	93.1	74.9
					265.1	258	280	82.9	14.9	0.96	0.00	20.6	0.00	6	4	2.140	0.617	0.711	3.13	84.0	85.1	5.4	211	−0.18	2.0	90.8	73.6
O	257	Southern chi Orionids	ORS	annual	250.1	230	280	78.8	17.7	0.87	0.05	26.8	−0.08	4	2.5	2.162	0.411	0.810	3.18	107.6	70.1	5.2	553	−0.32	2.1	94.5	75.6
O	97	Southern delta Cancrids	SCC	annual	287.1	270	310	117.5	16.1	0.97	−0.15	27.9	−0.01	3	3	2.298	0.399	0.826	3.48	108.3	107.1	4.8	266	−0.17	4.0	93.4	77.4
O	33	Northern iota Aquariids	NIA	annual	166.9	140	185	2.3	4.9	0.80	0.34	29.7	−0.08	6	4	1.795	0.273	0.848	2.41	306.2	166.9	5.1	215	−0.15	2.7	95.2	79.6
O	17	Northern Taurids	NTA	annual	218.8	200	225	49.7	20.7	0.87	0.23	29.1	−0.06	4	3	2.057	0.321	0.844	2.95	298.6	218.8	3.0	1188	−0.33	2.6	95.8	77.2
					236.2	225	258	63.7	23.7	0.82	0.14	27.1	−0.13	4	2.5	2.142	0.396	0.815	3.13	289.6	236.2	2.7	2170	−0.55	2.0	94.8	75.2
					263.9	258	270	87.4	26.4	1.07	0.02	23.8	−0.03	5	3	2.186	0.510	0.767	3.23	276.3	263.9	2.5	143	−0.06	2.7	92.0	74.6
	256	Northern chi Orionids	ORN	annual	267.9	240	290	97.4	25.2	1.00	−0.06	26.9	−0.03	3	3	2.196	0.413	0.812	3.25	287.3	267.9	2.4	401	−0.19	2.8	94.3	76.1
	1179	omega Geminids	OGE	annual	284.2	280	288	105.5	26.6	1.03	−0.05	22.0	0.01	3	2.5	2.240	0.581	0.741	3.35	267.9	284.2	2.8	39	−0.60		91.8	72.6
O	96	Northern delta Cancrids	NCC	annual	296.9	275	320	128.6	20.4	0.91	−0.23	28.2	−0.04	3	3	2.408	0.398	0.835	3.74	288.1	296.9	2.3	243	−0.10	2.9	93.2	78.0
O	11	eta Virginids	EVI	periodic	357.2	350	5	185.7	3.4	0.75	−0.27	27.3	−0.13	5	4	2.488	0.443	0.822	3.92	283.3	357.2	5.5	158	−0.74	1.9	91.6	74.2
	651	68 Virginids	OAV	annual?	18.5	10	26	201.7	−14.2	0.62	−0.36	27.0	−0.16	5	3	2.369	0.444	0.813	3.65	104.1	198.5	4.8	110	−0.33	2.2	93.0	79.5
O	21	alpha Virginids	AVB	annual	27.6	17	40	201.1	4.1	0.56	0.01	19.7	−0.17	4	1.5	2.709	0.717	0.735	4.46	250.9	27.6	7.1	104	−0.59		92.7	78.6
O	343	h Virginids	HVI	periodic	39.2	34	45	203.5	−11.1	0.27	−0.23	18.9	−0.29	3	2	3.072	0.750	0.756	5.38	65.9	219.2	0.7	61	−0.79		93.7	81.7
	47	mu Virginids	DLI	annual	37.3	30	47	226.8	−11.8	1.05	−0.27	29.3	0.08	4	2	2.435	0.371	0.848	3.80	292.2	37.3	6.6	68	−0.41		93.0	80.4
	150	Southern May Ophiuchids	SOP	annual	51.2	40	64	237.7	−24.2	0.78	−0.26	29.0	−0.15	4	2	2.522	0.383	0.848	4.01	113.9	228.0	4.7	114	−0.34	1.6	94.1	82.5
O	69	Southern mu Sagittariids	SSG	annual	85.9	71	98	271.2	−28.1	0.81	0.07	26.3	−0.09	14	4	2.605	0.468	0.820	4.21	101.5	265.9	4.7	73	0.01	3.0	94.1	84.6
O	164	Northern June Aquilids	NZC	annual	108.0	85	126	315.2	−3.5	0.83	0.29	38.9	−0.13	4	3	2.038	0.121	0.941	2.91	325.0	108.0	37.8	153	−0.75	2.4	94.8	84.6
O	165	Southern June Aquilids	SZC	annual	106.5	100	118	320.4	−26.5	0.99	0.27	39.9	−0.05	4	3	2.378	0.103	0.957	3.67	146.9	286.5	34.0	43	−0.73		94.8	86.5
O	5	Southern delta Aquariids	SDA	annual	129.6	122	145	342.1	−15.9	0.80	0.20	40.1	−0.20	3	2	2.512	0.087	0.965	3.98	149.7	309.6	26.6	2436	−0.92	3.8	95.6	86.5
	505	August iota Cetids	AIC	annual	154.5	140	168	3.2	−6.5	0.79	0.25	37.8	−0.13	3	2	2.246	0.116	0.948	3.37	145.1	334.5	20.0	139	−0.61		94.8	85.5
O	26	Northern delta Aquariids	NDA	annual	144.8	125	169	350.0	3.1	0.81	0.37	38.7	−0.10	3	2.5	2.232	0.097	0.957	3.33	328.3	144.8	21.1	355	−0.87	3.4	95.2	84.9
O	388	chi Taurids	CTA	annual	223.0	203	240	65.0	26.6	0.95	0.07	39.4	−0.08	6	5	3.122	0.116	0.963	5.52	323.4	223.0	15.4	154	−0.42	1.7	94.9	83.8
	253	December Canis Minorids	CMI	annual	273.8	250	310	121.2	11.4	1.00	−0.19	39.0	0.00	5	4	2.086	0.107	0.949	3.01	146.3	93.8	23.1	183	−0.63	2.4	95.6	83.4
	644	January lambda Leonids	JLL	annual	288.1	263	320	141.3	21.2	1.02	−0.34	39.7	0.04	3	3	1.865	0.081	0.957	2.55	331.4	288.1	21.8	172	−0.85	1.8	94.2	82.0
O	110	alpha Antliids	AAN	annual	311.1	302	317	157.1	−8.3	0.85	−0.37	44.9	−0.02	5	3	3.913	0.130	0.967	7.74	140.1	131.1	58.3	36	0.42		94.7	86.7
O	152	Northern Daytime omega Cetids	NOC	annual	53.6	44	61	17.1	19.9	0.75	0.41	40.3	0.12	6	5	2.173	0.096	0.956	3.20	31.4	53.6	40.2	12	−0.86		96.6	87.7
O	171	Daytime Arietids	ARI	annual	76.0	70	83	43.0	24.3	0.79	0.28	40.7	−0.02	3	2	2.641	0.078	0.970	4.29	29.0	76.1	27.5	28	−0.20		99.5	92.8
O	172	Daytime zeta Perseids	ZPE	2010, 2017	77.5	74	80	60.7	22.3	1.89	−1.22	28.5	−0.13			1.866	0.319	0.829	2.55	59.1	77.5	2.3	3	1.09		94.8	90.3
O	221	Daytime Sextantids	DSX	annual	189.7	184	196	157.4	−2.7	0.40	−0.42	32.5	−0.17	4	3	1.127	0.144	0.872	1.20	213.0	9.7	24.2	23	−0.85		97.5	86.3
O	320	omega Serpentids	OSE	annual	276.3	274	280	251.7	−5.2	0.63	−0.09	43.3	−0.26	3	2.5	10.074	0.176	0.982	31.97	48.9	276.3	45.2	8	−0.72		105.0	92.5
O	9	October Draconids	DRA	annual	194.1	191	198	262.5	55.0	0.24	0.56	19.6	0.20	5	2	2.880	0.996	0.654	4.89	173.0	194.1	30.0	13	0.13		92.6	84.8
	525	iota Cygnids	ICY	annual	219.1	210	230	297.4	53.8	0.38	0.37	16.9	0.02	8	2	2.898	0.987	0.659	4.93	188.8	219.1	24.6	52	−0.29		86.9	74.0
O	10	Quadrantids	QUA	annual	283.4	278	289	230.0	49.8	0.86	−0.09	40.7	−0.17	5	2.5	2.872	0.979	0.659	4.87	172.4	283.4	71.2	2171	−0.90	2.6	98.9	86.9
O	334	December alpha Draconids	DAD	annual	250.9	230	265	203.0	62.3	1.04	−0.55	41.2	0.00	6	3	2.699	0.975	0.639	4.43	185.8	250.9	72.9	487	−0.58	2.0	97.2	86.5
	574	gamma Ursae Majorids	GMA	annual	245.1	240	250	184.1	52.1	1.03	−0.27	52.4	−0.01	3	2.5	3.346	0.986	0.705	6.12	179.4	245.1	97.3	15	−0.03		100.4	91.6
O	15	Ursids	URS	annual	269.9	267	272	218.1	76.4	1.11	−0.32	33.2	−0.10	3	2	5.775	0.935	0.838	13.88	206.8	269.9	52.5	700	−0.44	2.0	101.0	87.9
O	404	gamma Ursae Minorids	GUM	annual	299.7	296	305	229.0	67.7	0.99	−0.70	29.4	0.15	5	2	2.792	0.952	0.659	4.67	203.1	299.7	48.0	60	−0.49	1.4	93.4	77.9
O	12	kappa Cygnids	KCG	periodic	140.4	120	155	286.1	49.1	0.56	0.89	22.6	0.20	10	3	3.524	0.968	0.725	6.62	206.2	140.4	34.0	289	−1.33	1.5	94.3	80.8
	757	chi Cygnids	CCY	periodic	168.6	160	178	302.0	28.4	−0.32	1.11	15.2	0.01	4	2.5	2.867	0.937	0.673	4.86	213.5	168.6	17.3	46	−0.75		88.1	75.6
O	197	August Draconids	AUD	annual	149.0	125	170					21.0	−0.01		3	3.006	1.001	0.667	5.21	184.6	149.0	32.8	379	−0.67	2.3	92.5	78.1
	1044	epsilon Ursae Minorids	EPU	2019	181.9	181	183	255.0	82.6	−3.35	−0.41	33.6	0.21	3	1	2.756	1.003	0.636	4.58	178.7	181.9	57.8	10	−0.83		89.2	79.7
O	18	Andromedids	AND	annual	231.1	212	255	21.7	33.5	0.14	0.78	17.2	−0.11	5	2	3.024	0.798	0.736	5.26	236.5	231.1	10.5	227	0.07	2.5	93.0	83.1
O	446	December phi Cassiopeiids	DPC	2011	252.2	251.7	252.9	19.6	57.7	−0.87	0.87	16.4	0.23	2	2	3.030	0.897	0.704	5.28	218.6	252.2	18.0	18	−0.31		95.0	83.7
	456	May psi Scorpiids	MPS	annual	67.6	50	88	246.9	−9.5	0.56	0.21	23.8	−0.21	4	2	2.773	0.582	0.790	4.62	267.8	67.6	9.2	160	−0.55	1.9	93.0	79.6
O	61	tau Herculids	TAH	annual	84.4	81	88	230.4	44.8	−0.33	−0.06	14.2	−0.13	4	1.5	2.663	1.003	0.623	4.35	194.1	84.4	19.1	18	−0.54		87.6	73.6
O	170	June Bootids	JBO	2010	92.5	85	93	225.8	47.5	−0.80	−0.02	14.2	0.01	2	1	3.001	1.012	0.663	5.20	187.6	90.1	18.9	9	−0.41		89.3	79.1
	459	June epsilon Ophiuchids	JEO	2019	92.9	92.4	93.4	245.7	−7.8	−0.02	0.35	13.7	−0.22	0.5	1	2.625	0.891	0.661	4.25	226.4	92.9	5.2	12	−1.07		90.2	76.6
O	254	Phoenicids	PHO	2019	232.2	230.4	233.7	6.7	−7.7	0.08	−0.54	10.9	0.47	2	1.5	3.243	0.946	0.708	5.84	26.6	52.2	2.7	9	−1.57		88.0	72.8
O	323	xi Coronae Borealids	XCB	annual	294.3	289	297	249.5	30.0	0.64	−0.20	45.9	0.11	4	2.5	5.207	0.789	0.848	11.88	124.7	294.3	78.5	44	−0.14		96.7	87.9
O	338	omicron Eridanids	OER	annual	230.5	210	255	57.7	−1.2	0.67	−0.18	28.0	−0.16	6	3	4.037	0.512	0.873	8.11	91.9	50.5	19.3	381	−0.75	2.2	96.8	79.2
	709	lambda Canis Majorids	LCM	annual	273.3	250	296	88.8	−22.5	0.84	−0.78	25.1	0.07	3	3	4.565	0.779	0.829	9.75	56.6	93.3	29.2	192	−0.16	2.4	96.7	82.0
	341	January xi Ursae Majorids	XUM	annual	298.4	296	301	169.5	32.8	0.51	−0.43	41.3	0.11	3	1.5	1.530	0.222	0.855	1.89	312.9	298.4	68.0	131	−1.20	1.9	92.6	79.6
O	346	x Herculids	XHE	annual	351.0	348	355	253.6	49.1	1.09	−0.38	34.7	−0.04	4	2	2.821	0.977	0.654	4.74	196.7	351.0	59.2	36	−0.70		95.7	81.2
O	526	Southern lambda Draconids	SLD	annual	221.8	220	224	161.8	68.0	0.15	−0.83	49.3	0.59	6	2	4.281	0.985	0.770	8.86	190.1	221.8	88.7	40	−0.86		107.7	94.6
	746	e Velids	EVE	annual	251.5	241	264	131.0	−46.3	0.73	−0.29	42.5	0.01	6	1	2.657	0.978	0.632	4.33	7.2	71.5	75.8	95	−0.63	2.5	100.7	92.8
O	63	Corvids	COR		Cannot confirm existence.																						
O	137	pi Puppids	PPU		Radiant position exists in difficult area by Japanese latitude TV observation.																						
O	233	October Capricornids	OCC		Cannot confirm existence.																						

2012. Alpha Capricornids consist of three components from the radiant drift study (Ueda, 2019). Jenniskens et al. (2016a) described that it consists of two showers alpha Capricornids and xi2 Capricornids (#623 XCS). Variations in radiant position and geocentric velocity for the selected alpha Capricornids are shown in Figure 2. The characteristics in Figure 2 change at 120° solar longitude. Before 120° corresponds to #623 xi2 Capricornids (Jenniskens et al., 2016a). After 132° solar longitude a small change in characteristics is also found. I considered all these components as indicating alpha Capricornids interior structures. Epsilon Aquariids (#692 EQA) is a possible end part of this shower.

3.2.2 Taurid Complex

Long term active duration meteor shower group whose radiant position exists on both sides of the ecliptic plane. Thus, radiant positions are $175° < \lambda - \lambda_\odot < 200°$, and $3° < |\beta| < 15°$. Perihelion distance is about 0.4 AU. Northern iota Aquariids in August are the first sure Taurid complex member. In January, northern and southern delta Cancrids are a certain ending part of the Taurid complex.

*** Southern Taurids (002#STA)–resonance component**

This Southern Taurid component is in mean motion resonance with Jupiter (Asher & Izumi, 1998; Shiba, 2016). Table 2 data were derived from 2008, 2012, 2015 and 2018 data that unfortunately included some non-resonance (= annual) component meteors, so that the results contain a few minor discrepancies. Comparing with the annual component, differences are: short active duration (three weeks); 0.9 average magnitudes brighter because the resonance component contains many bright meteors; perihelion longitude does not progress but stays close to 158°; and especially highly concentrated radiants (Figure 3a–c).

*** Southern Taurids (002#STA)–annual component**

Table 2 data were derived from years free from the resonance component, 2007, 2009, 2010, 2011, 2013, 2014, 2016, 2017, 2019 and 2020. I presume the long term active season starts at 187° solar longitude. Southern delta Piscids (#216 SPI) may be the early part of STA. The end part overlapped with Southern chi Orionids (#257 ORS) with indistinct boundaries; as a result, it is difficult to determine which individual meteor belongs to which shower. Activity features indicate a varying complex along with long term activity that suggests some meteor showers combined (Figure 3d–f). Table 2 data are divided based on where characteristics change with solar longitude. Nu Piscids (#627 NPS), Southern October delta Arietids (#28 SOA), xi Arietids (#624 XAR) fall within the 187–213° meteor shower. Lambda Cetids (#626 LCT), s Taurids (#628 STS), f Taurids (#637 FTR), lambda Taurids (#625 LTA) fall within the 213–231° meteor shower. Omega Taurids (#286 FTA) fall within the 231–258° meteor shower. Meteor shower members in that last interval characteristically contain bright meteors.

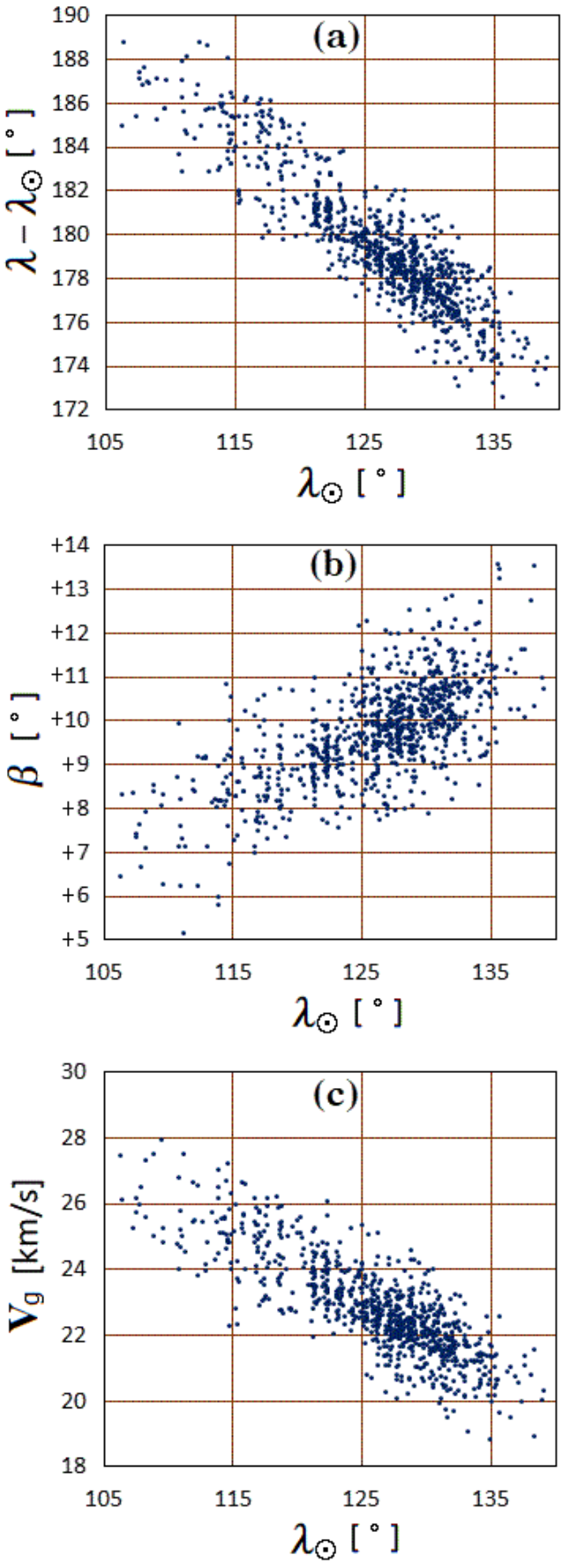

Figure 2 – Radiant position and V_g drift of CAP.

*** Southern chi Orionids (#257 ORS)**

The radiant point appears about 8° east of the STA (annual) position at the final stage of STA. Southern

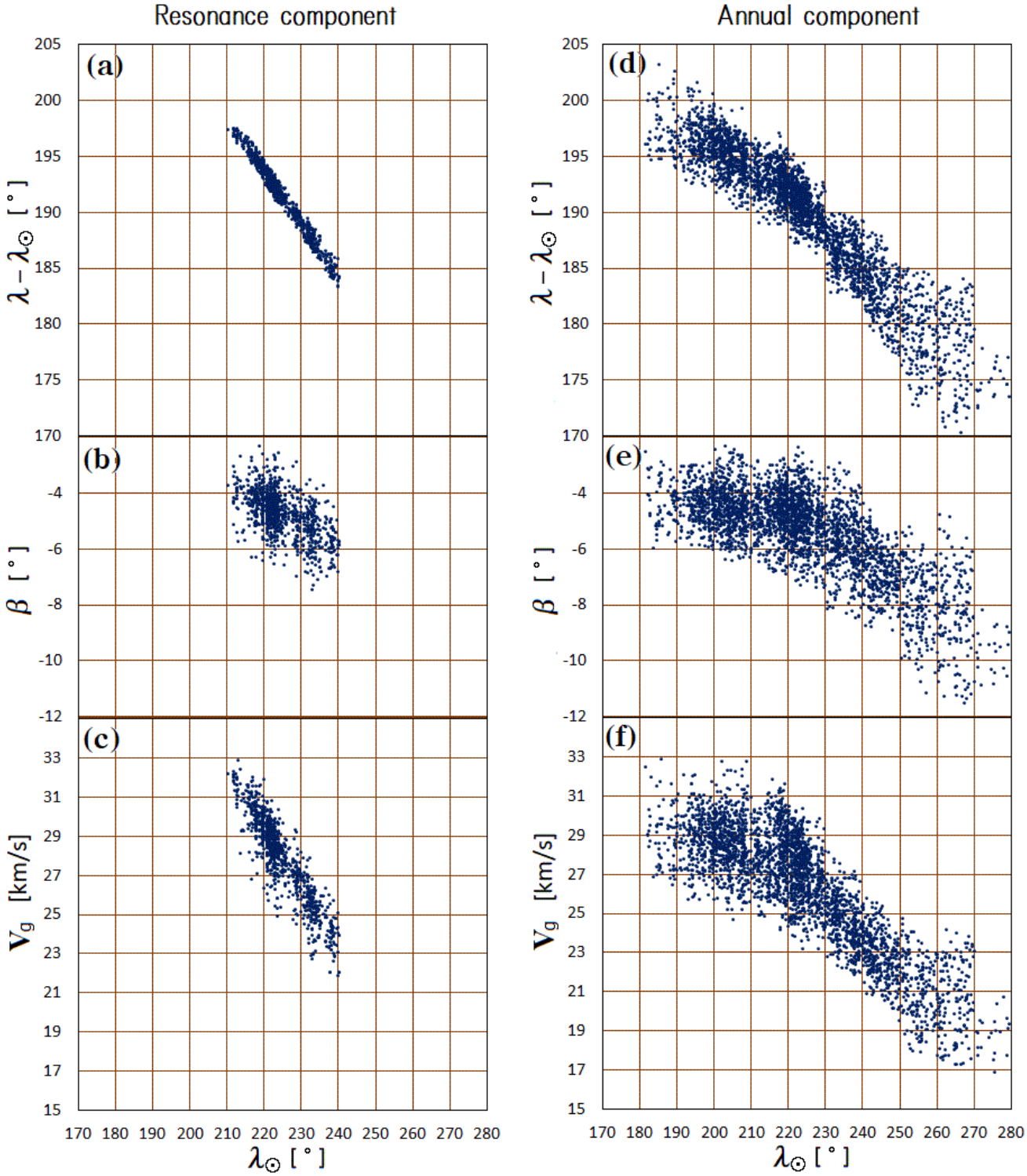

Figure 3 – Radiant position and V_g drift of Southern Taurids.

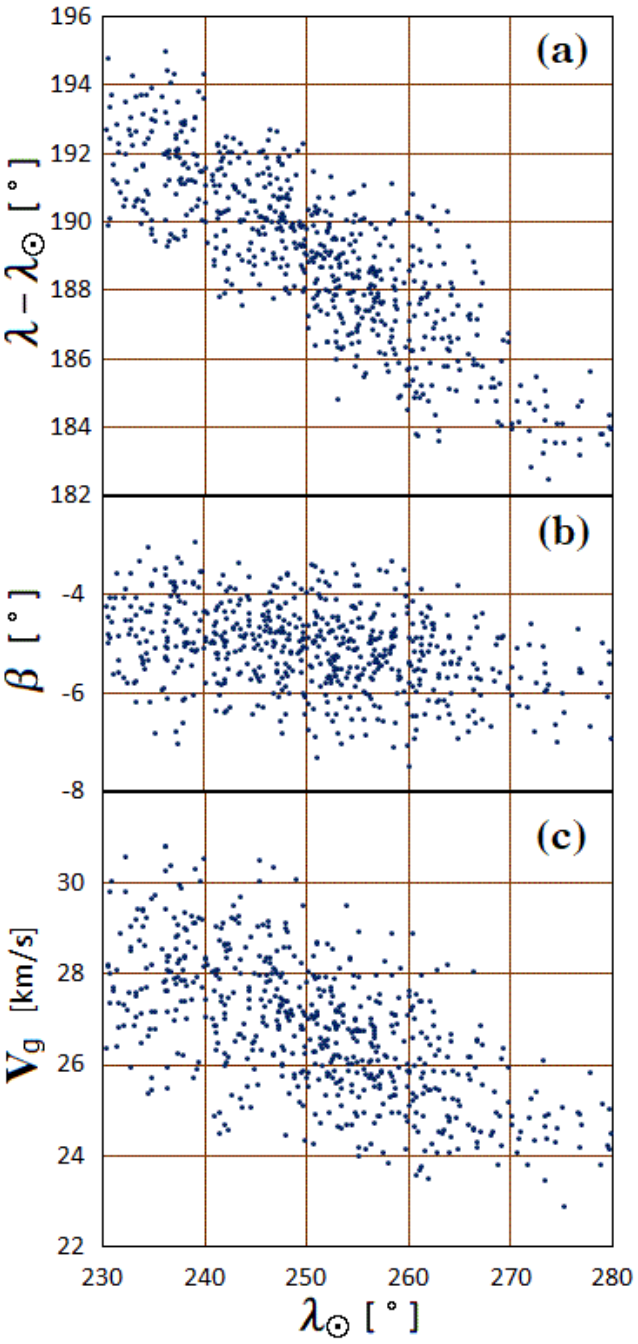

Figure 4 – Radiant position and V_g drift of southern chi Orionids.

delta Cancrids (#97 SCC) start and overlap from east of the ORS radiant region at the final stage of ORS (Figure 4). For many meteors in the ORS peripheral region it cannot be judged which meteor showers they belong to. Table 2 data are somewhat similar to m Taurids (#636 MTA). The final part falls under December zeta Taurids (#638 DZT) that continue after ORS.

*** Southern delta Cancrids (#097 SCC)**

Southern and northern delta Cancrid orbits are especially similar. If we judged using the D criterion with $D_d < 0.105$, many meteors would be selected belonging to both southern and northern showers. Observable SCC meteors are fewer than northern delta Cancrids. Radiant drift speed is faster than ORS (Table 2: dα column) and the same as the motion of the solar longitude

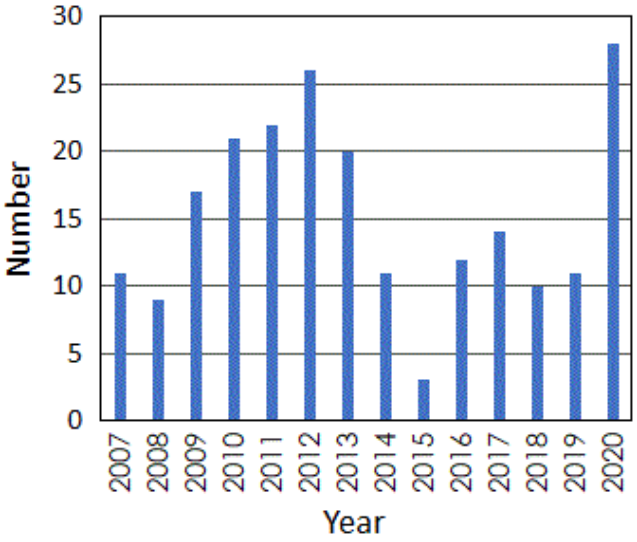

Figure 5 – Number of NIA meteors in each year.

(360/365.25 = 0.986). These features suggest a transient stage from the Taurid complex to the Antihelion meteor source.

*** Northern iota Aquariids (#033 NIA)**

Solar longitude in Table 2 data is about one month later than the general NIA maximum but similar to northern delta Piscids (#215 NPI). I adopted the smaller IAU MDC meteor shower number NIA in this paper. NIA to NPI activity continues smoothly with no clear boundary, which indicates a single meteor shower feature. After NIA decreases, northern Taurids appear. The early season NIA perihelion distance was small, because it may be an effect of contamination by the northern delta Aquariids (#26 NDA). Meteor numbers vary significantly from year to year (Figure 5). A reason would be the influence of the weather; however, the low number in 2015 cannot be explained by only bad sky conditions.

*** Northern Taurids (#017 NTA)**

The beginning of the long term active season till 214° is a transition term from the ending of the northern iota Aquarids, and after 255° is the transition term to northern chi Orionids (Figure 6). This shower's long term duration was calculated divided into three periods. Northern October delta Arietids (#25 NOA), delta Arietids (#631 DAT) and tau Arietids (#630 TAR) fall within the 200–225° meteor shower. November eta Taurids (#632 NET), A1 Taurids (#635 ATU), A2 Taurids (#629 ATS), p Taurids (#633 PTS) and tau Taurids (#634 TAT) fall within the 225–258° meteor shower. Radiant ecliptic longitude λ and ecliptic latitude β are linear with solar longitude $\lambda_\odot$ on the whole period ($214 < \lambda_\odot < 265$):

$$\begin{aligned} \lambda &= 0.76(\lambda_\odot - 232.^\circ 18) + 63.^\circ 00 \\ \beta &= 0.01(\lambda_\odot - 232.^\circ 18) + 2.^\circ 49 \\ V_g &= -0.13(\lambda_\odot - 232.^\circ 18) + 27.6 \quad [\mathrm{km/s}]. \end{aligned}$$

*** Northern chi Orionids (#256 ORN)**

The ORN radiant distribution superposed on the last stage of NTA are shown together in Figure 7. ORN

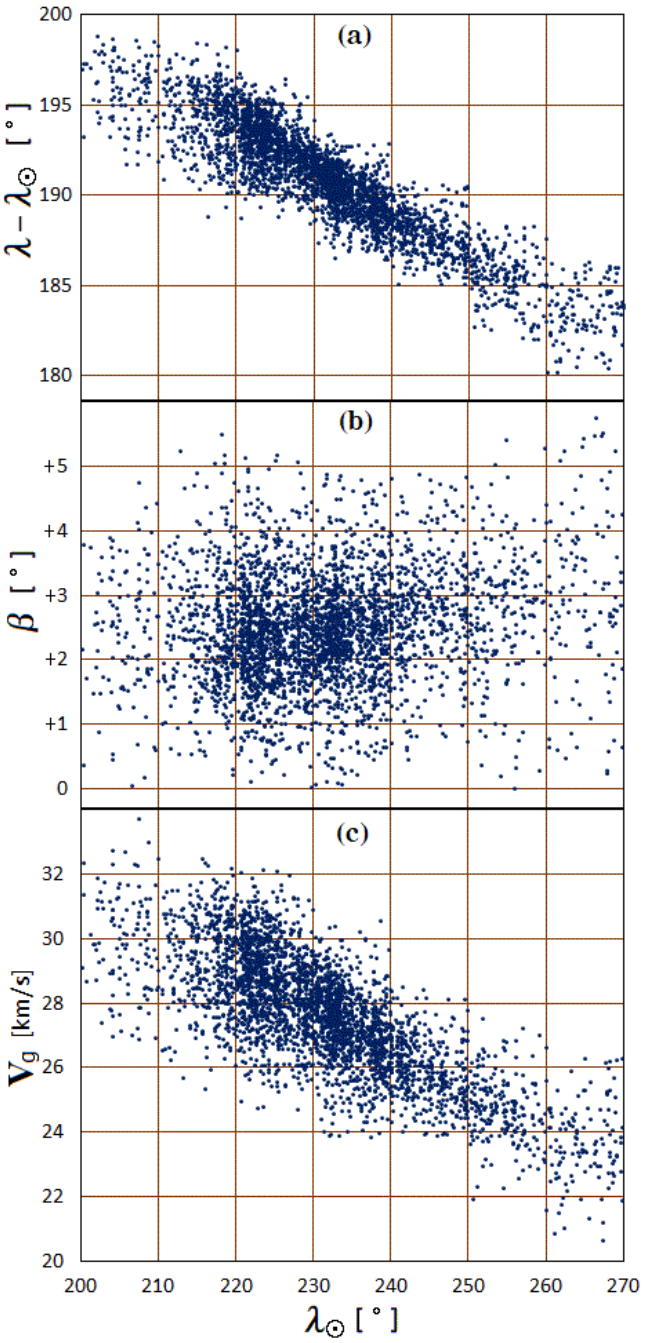

Figure 6 – Radiant position and V_g drift of Northern Taurids.

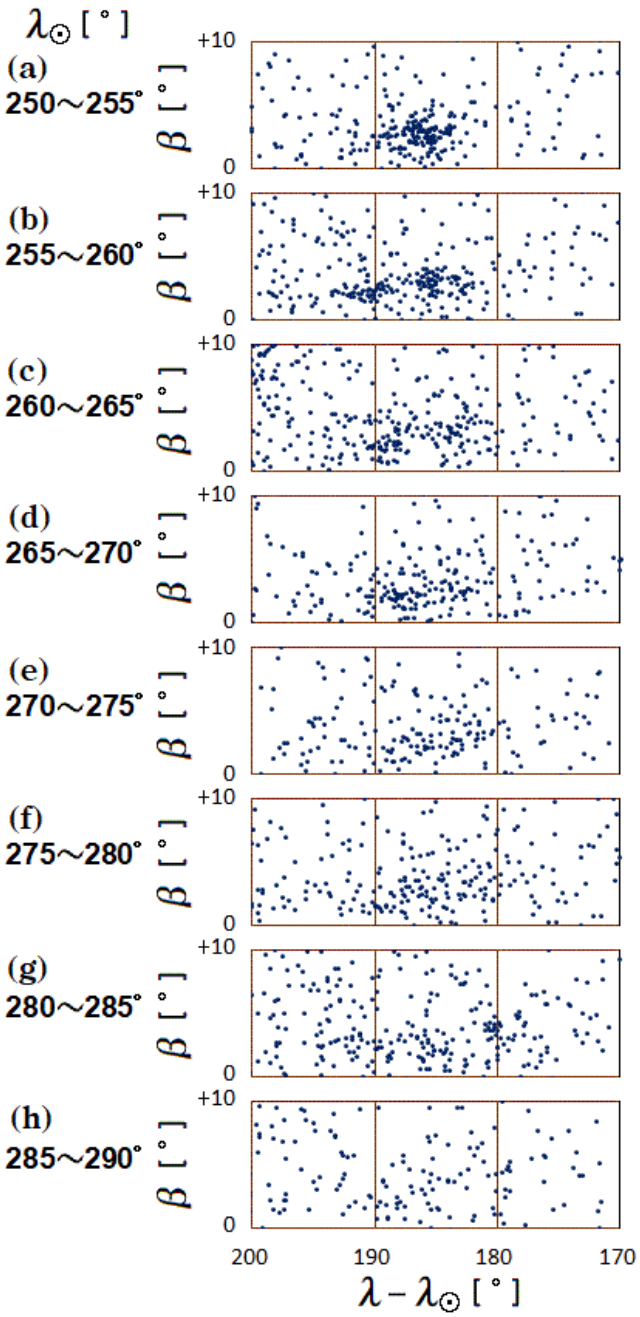

Figure 7 – Radiant distribution of late Northern Taurids and Northern chi Orionids area.

appears to the east of NTA ($\lambda - \lambda_\odot = 190°$) at solar longitude 255° (Figure 7b). However, both showers come together after solar longitude 265° (Figure 7d). December epsilon Geminids(#726 DEG) correspond to the two meteor showers' combined periods.

*** omega Geminids (#1132 OGE)**

This new shower found in Figure 7(g) at $\lambda - \lambda_\odot = 180°$ corresponds to the NTA drifted location. However, between the NTA and this new shower exists a gap in the active duration, so I describe it in this paper as a new shower. It is an annual meteor shower.

*** Northern delta Cancrids (#096 NCC)**

In Figure 7(g), at $\lambda - \lambda_\odot > 190°$, the sparsely concentrated radiants are presumed to be the NCC initial stage. Activity level decreases by about half between 300–305° solar longitude. Bright meteors are few, similar to SCC.

3.2.3 February to June ecliptic meteor showers

Some meteor showers exist between February and June in the corresponding area to the Taurid complex radiant, but these all are faint showers.

*** eta Virginids (#011 EVI)**

A four-year cycle in activity enhancement was found, in accordance with an expected resonance with Jupiter's orbital period (Shiba, 2018). So I derived Table 2 data based on six years' data, 2009, 2010, 2013, 2014, 2017 and 2018. The Northern March Virginids (#123 NVI) (Sekanina, 1973) may be a corresponding meteor shower but the velocity is not equal.

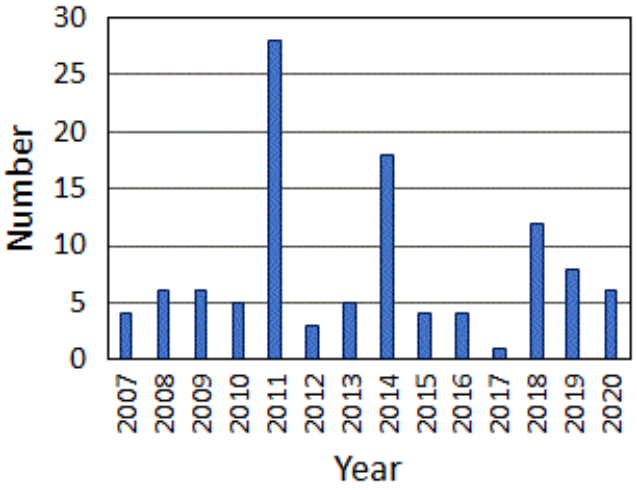

Figure 8 – Number of OAV meteors in each year.

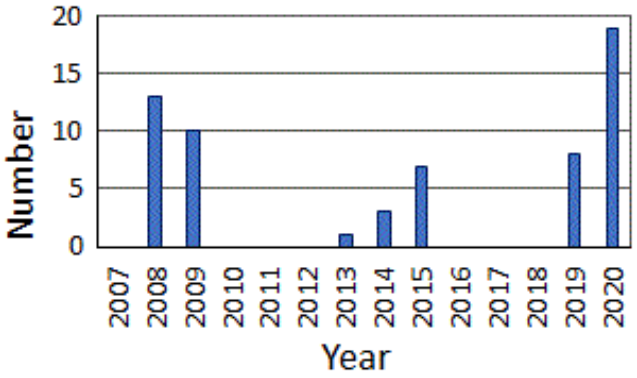

Figure 9 – Number of HVI meteors in each year.

*** 68 Virginids (#651 OAV)**

Meteor shower characterized by sparse radiants. Outbursts were observed definitely in 2011 and 2014 but meteors were scarce in other years (Figure 8). This feature is difficult to explain by weather conditions. Lambda Virginids (#49 LVI) orbit exists in the mirror position in the ecliptic plane.

*** alpha Virginids (#021 AVB)**

Meteor numbers are few but appears to be a stable annual meteor shower. Sigma Leonids (#136 SLE) is between meteor showers EVI and AVB in terms of their season and position. If SLE is confirmed as annual meteor activity, it may be the pre-meteor shower of AVB. Daytime psi Virginids (#240 DFV) is a possible twin shower of AVB.

*** h Virginids (#343 HVI)**

Orbit shape is similar to AVB but inclination about 0°. The yearly meteor numbers are shown in Figure 9. It indicates a six year cycle in activity. Semi major axis vs solar longitude is shown in Figure 10 and indicates no correlation, which is to say, meteor periods are constant with solar longitude. The calculated meteor orbital period is 5.4 years which indicates 1:2 resonance with Jupiter. 68 Virginids (#651 OAV) radiant appears near same position three weeks before, however no periodic activity was observed.

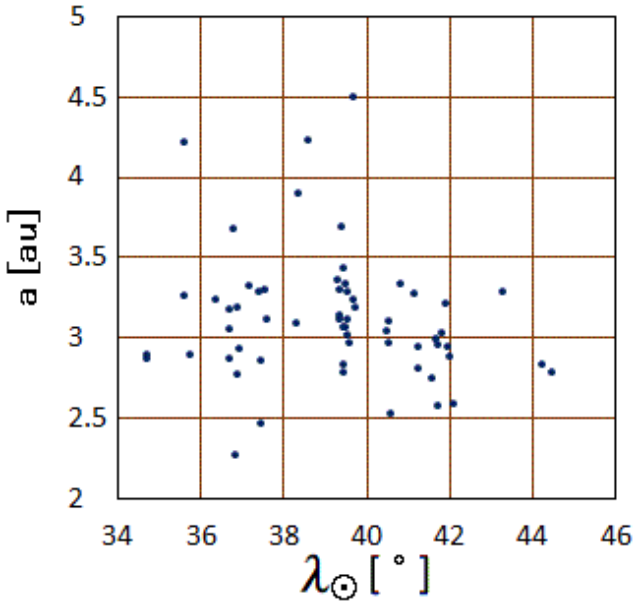

Figure 10 – HVI semi major axis as a function of solar longitude.

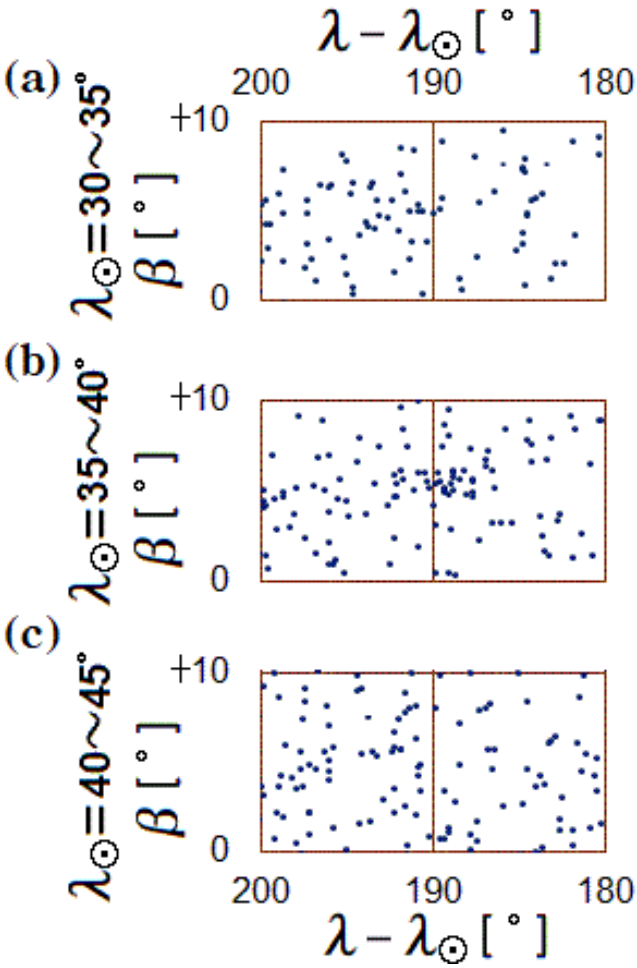

Figure 11 – DLI radiant area.

*** mu Virginids (#047 DLI)**

Radiant distribution is shown in Figure 11. Many meteor showers are identified in this area that require careful identification. Gamma Librids (#139 GLI) is a corresponding radiant position but a different velocity.

Northern May Ophiuchids (#149 NOP) and xi Scorpiids (#920 XSC) are close radiant positions to this shower but observable 2–3 weeks later.

*** Southern May Ophiuchids (#150 SOP)**

Indistinct radiant concentration meteor shower. Iota1 Librids (#826 ILI) may be a related meteor shower that appears one month before. Removed meteor shower #55 ASC is possibly the same meteor shower.

*** Southern mu Sagittariids (#069 SSG)**

It is a very faint meteor shower and there is an unclear boundary with sporadic meteors. Many faint meteors included and luminous endpoint is high. Peripheral radiant area ($0.105 > D_d > 0.0525$) is moreover 0.2 magnitudes fainter than central area ($D_d < 0.0525$). Southern sigma Sagittariids (#168 SSS) is a possible corresponding shower. Southern May Ophiuchids (#150 SOP) is a possible pre-meteor shower but activity level decreases between both showers around solar longitude = 75–79°.

3.2.4 Antihelion group

This group's radiant positions exist between $\lambda - \lambda_\odot$ = 200–215°, and β = 3–13° both north and south. Perihelion distance is very close to the Sun, approximately 0.1 AU. Only SDA shows a distinct maximum but other meteor showers have an indistinct maximum and sparse distribution of radiants or orbits. Every shower has a wide inclination distribution.

*** Northern June Aquilids (#164 NZC)**

Distinct activities including many meteors were observed only in 2011 and 2018 because these years had clear sky conditions. Semi major axis and inclination are decreasing over the long term active duration. Aquilids (#1111 AQI) will be corresponding to this shower.

*** Southern June Aquilids (#165 SZC)**

The radiant point exists in Capricornus not in accord with the name. Table 2 data almost agree with Jenniskens (2016a). In 2016, rather many meteors appeared ($N = 11$). Microscopiids (#370 MIC) will correspond to this meteor shower and are a more suitable name I think. SDA activity starts on the north side of this shower after it has disappeared.

*** Southern delta Aquariids (#005 SDA)**

SDA radiant distribution is shown in Figure 12 for every 5° solar longitude bin. The area of radiant concentration moves slowly to the southwest. Unusual variations occur after its maximum. The radiant distribution extends east-west after 130° solar longitude (Figure 12d). New radiant components develop on the northeast side after 140° solar longitude (Figure 12f). Original components disappear after 150° (Figure 12h). I judged the original component is SDA and later component on the northeast side is August iota Cetids (#505 AIC). August omicron Aquariids (#640 AOA) (Jenniskens et al., 2016a) will come under the SDA and AIC combined active period however I could not identify that meteor shower in this study.

*** August iota Cetids (#505 AIC)**

Radiant position drift and orbit are similar to SDA, so the two meteor showers may share a common origin or evolution. Weak activity continues to about 170° solar longitude. The inclination and perihelion distance of both showers are shown in Figure 13. Many meteors are identified clearly as SDA by their radiant positions, however some of their inclinations between 140–150° solar longitude indicate an intermediate feature with AIC (Figure 13a). On the other hand, the perihelion distance feature indicates the existence of an obscure gap between the two showers (Figure 13b). This transition period corresponds to August omicron Aquariids (#640 AOA). The terminal phase of AIC corresponds to phi Cetids (#642 PCE).

*** New shower**

A small meteor shower is found southeast of SDA at solar longitude 130–140° (Figure 12d,e). With semi major axis over 6 AU, it is a Halley type meteor shower, so that it is not described in Table 2.

*** Northern delta Aquariids (#026 NDA)**

Radiant distribution for 5° solar longitude bins is shown in Figure 14. Interestingly in this plot the major axis of the NDA radiant distribution rotates clockwise as solar longitude increases. The orbit is almost a mirror image of AIC in the ecliptic plane. Inclination starts to vary significantly after 140–145° solar longitude (Figure 15). Northern iota Aquariids (#033 NIA) appear southwest of NDA after 150° solar longitude (Figure 14f).

*** chi Taurids (#388 CTA)**

A sparse radiant distribution exists to the east of NTA. D_d criterion distributions for Antihelion meteor showers are shown in Figure 16. If orbit distributions are sparse, symbols will be plotted higher towards the right side of the figure. The SDA meteor shower, whose orbits are highly concentrated, shows symbols distributed almost horizontally. CTA shows the broadest orbit distribution characteristic in all the Antihelion meteor showers (Figure 16). The inclination has a broad distribution 4–25°. A smaller semi major axis than Jenniskens (2016a) is determined, a possible reason being that adopted radiant concentration positions do not correspond. Sigma Arietids (#237 SSA) may be the initial part, but the inclination has differences. 55 Arietids (#538 FFA) may also correspond to the earlier half, but the perihelion distance is larger.

*** December Canis Minorids (#253 CMI)**

Radiants and orbits are sparse (Figure 16). Perihelion distance variation changes from increasing to decreasing at 275° solar longitude (Figure 17). 68 Geminids (#610 SGM) is about 10 days early but a possible corresponding shower. The perihelion distance decrease after 275° solar longitude (Figure 17) corresponds to the

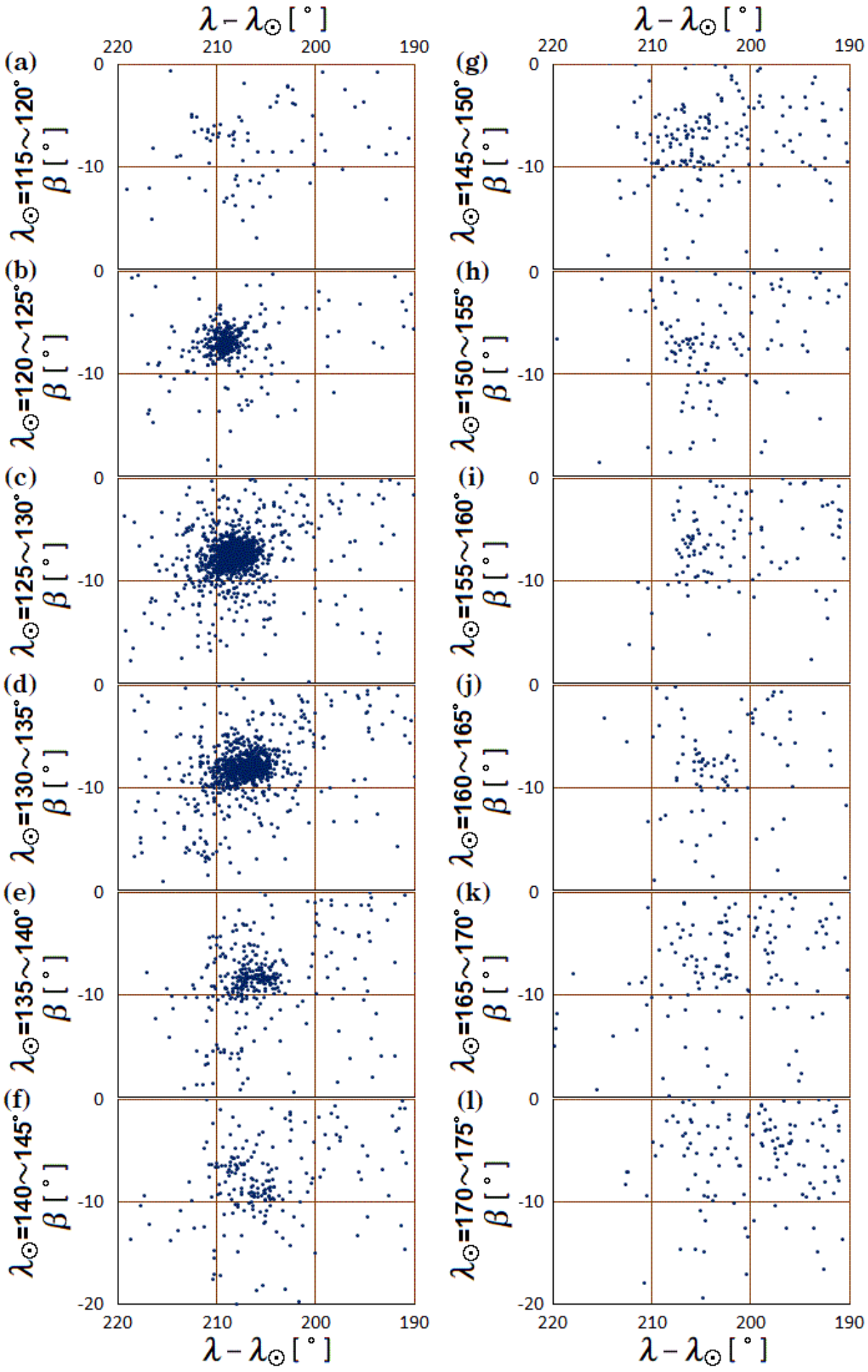

Figure 12 – Radiant distribution of SDA area.

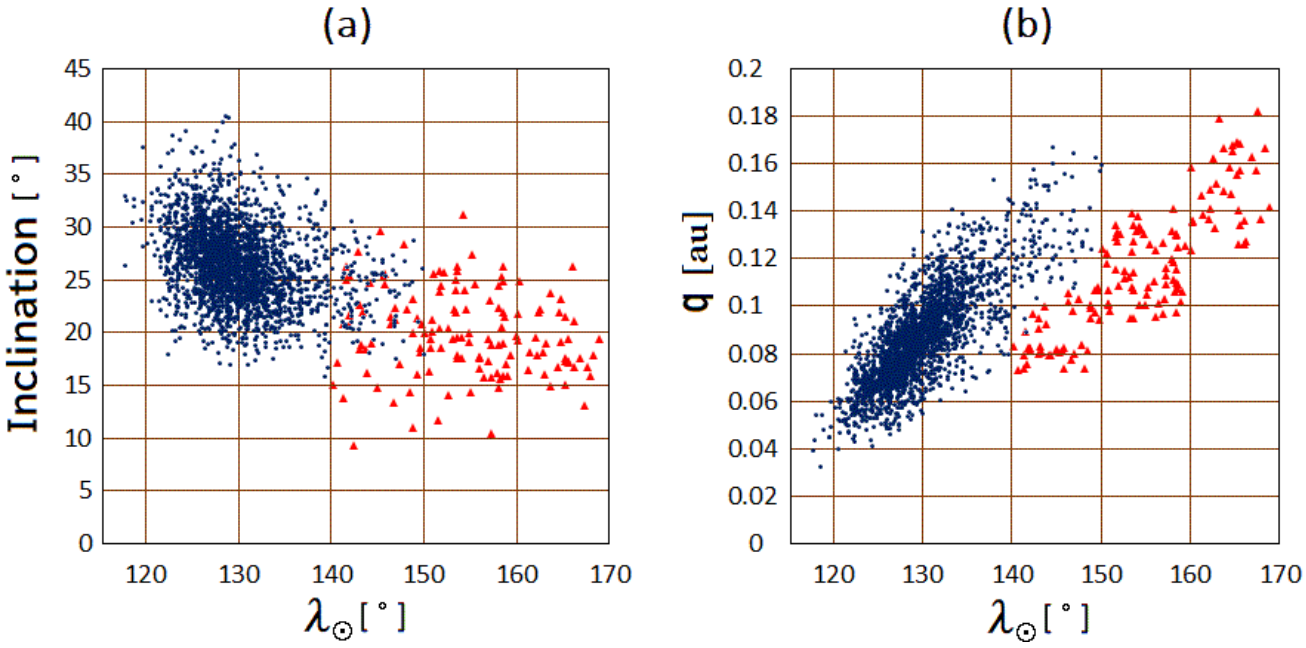

Figure 13 – Inclination and perihelion distance distribution of SDA (blue dots) and AIC (red triangles).

omicron Leonids (#515 OLE). The orbit of #644 JLL below is the mirror image of this shower in the ecliptic plane.

*** January lambda Leonids (#644 JLL)**

A sparse radiant distribution meteor shower appears to the south of Geminids at its ending stage. Activity duration is long and concentration of orbits is at a low level. January kappa Leonids (#747 JKL) is apparently the same as this shower. Iota Leonids (#710 IOL) and January theta Leonids (#748 JTL) correspond with the ending part of this shower. December rho Geminids (#641 DRG) may correspond with beginning part of this shower but with a rather different orbit.

*** alpha Antliids (#110 AAN)**

The observed number of meteors is very few, six meteors in 2020 at maximum, but the meteor shower certainly exists. Radiant position is near the Sextans–Hydra border but not Antlia.

3.2.5 Daytime meteor showers

This group's radiant position is near the Sun, therefore many meteor showers cannot be observed by optical techniques. Even so, some showers do have a short observable time in twilight by TV observation. Most of these meteor showers' orbits have similar characteristics as the Antihelion group. Belonging to either group is determined by the ascending node or descending node intersecting with the Earth. If perihelion longitude is approximately 90 or 270°, we can observe twin showers, but no such pair is found in Table 2. Radio observation results in a tendency for shorter orbital periods than optical observations. It may indicate that fine meteoroid particles have a shorter orbital period.

*** Northern Daytime omega Cetids (#152 NOC)**

Radiant exists in a barely observable position that is in Pisces but not in Cetus. Observable time is only one hour or less per day.

*** Daytime Arietids (#171 ARI)**

Identifying the results for this meteor shower by radiant position and V_g does not lead to good agreement with D criterion results. The reason depends on the wide variation in orbital inclination. Luminous beginning and end heights are at high altitude where meteoroids are estimated easily to break. June epsilon Arietids (#680 JEA) is apparently the ending stage of this shower.

*** Daytime zeta Perseids (#172 ZPE)**

The radiant position is closer to the Sun than ARI and all the observable time is in morning twilight. Only one meteor was observed in 2010 and two in 2017. Two radiant points are in the north, 4°.5 from the ecliptic plane, another one 4°.5 south. If we accumulate observation data, this shower may divide into two showers. Daytime epsilon Arietids (#154 DEA) is a possible precursor of this shower, but between the two showers activity discontinues. Orbit indicates Taurid Complex membership but not Antihelion type.

*** Daytime Sextantids (#221 DSX)**

Especially small semi major axis orbit and not close to Jupiter's orbit. Observed number of meteors is few but it is a meteor shower with highly concentrated orbits.

*** omega Serpentids (#320 OSE)**

Large and dispersed semi major axis values calculated from a small number of meteors that indicates

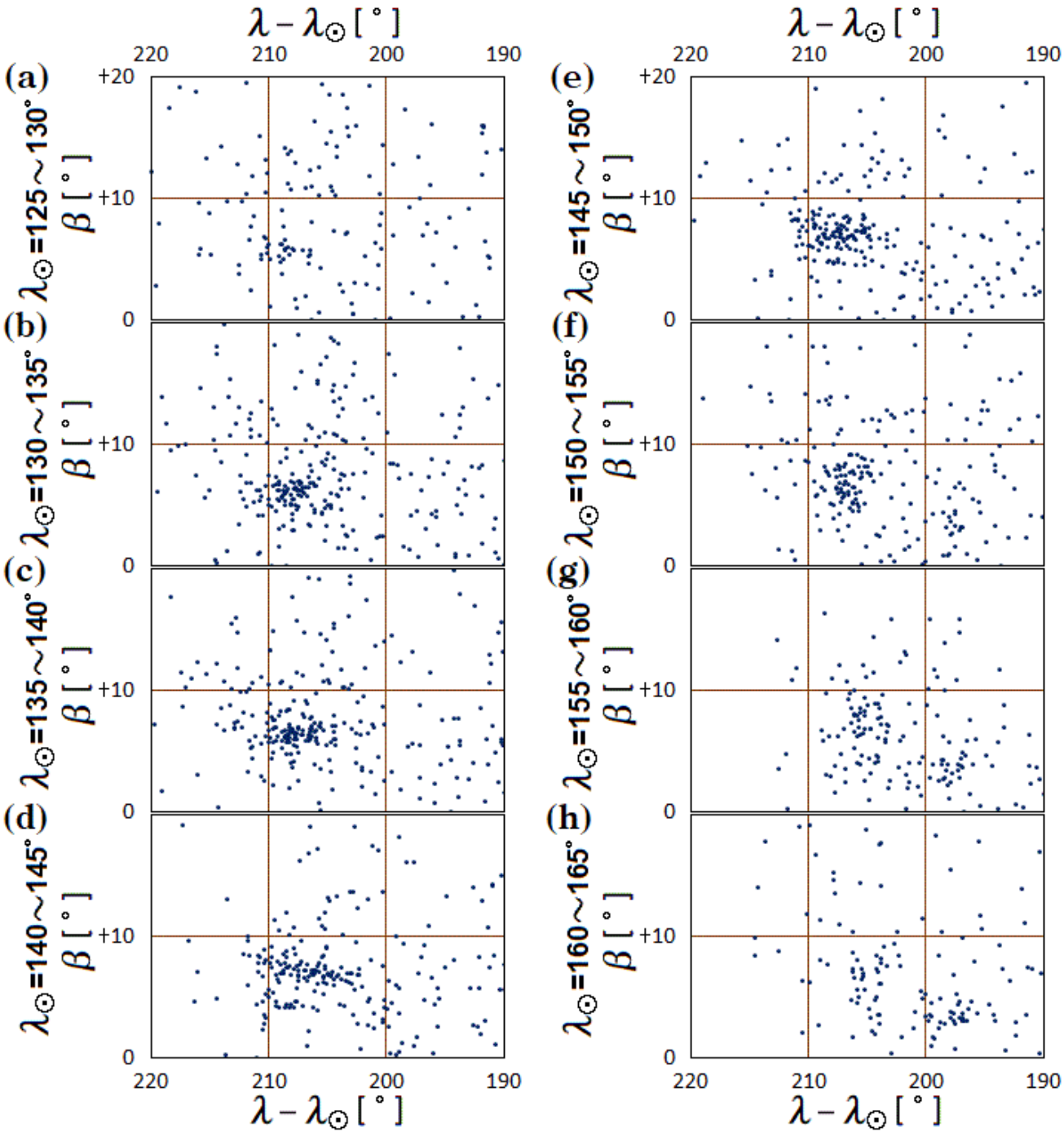

Figure 14 – Radiant distribution of NDA area.

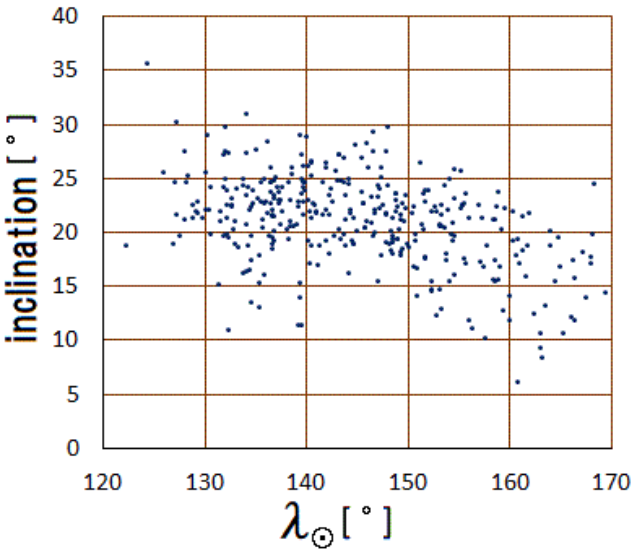

Figure 15 – NDA inclination as a function of solar longitude.

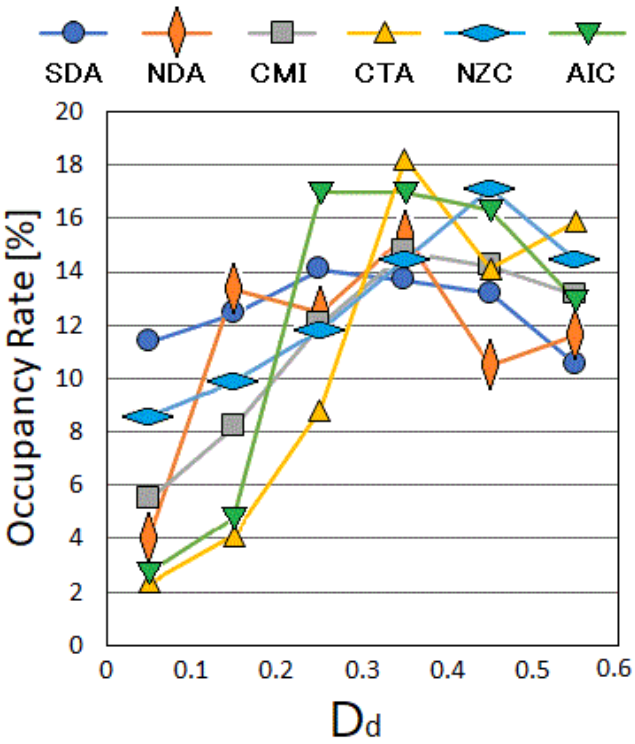

Figure 16 – D criterion distribution for Antihelion showers.

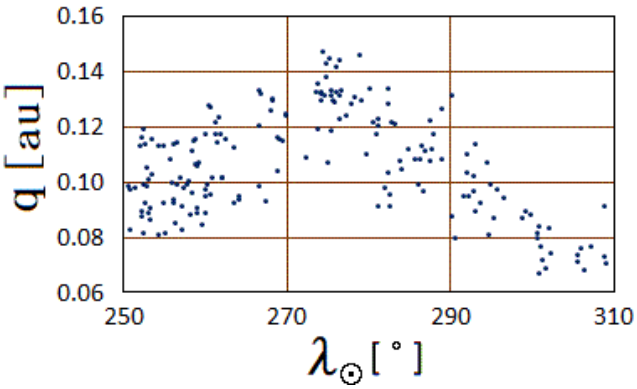

Figure 17 – CMI perihelion distance.

Halley type meteor shower. Long mean luminous duration, over one second, allows derivation of the influence of deceleration by the atmosphere, which would be enormous. Sigma Serpentids (#330 SSE) apparently corresponds to this shower. I think it is not suitable that both OSE and SSE are listed as established meteor showers.

3.2.6 October Draconids and iota Cygnids

*** October Draconids (#009 DRA)**

Only a total of three meteors were recorded in each of 2009 and 2018. There were only a few DRA meteors because, containing many faint meteors, the shower is difficult for TV observations. Luminous height is especially high.

*** iota Cygnids (#525 ICY)**

Geocentric velocity is slow and radiant points are sparse. The orbit shape is similar to October Draconids however the orbit direction differs ($D_d = 0.16$). Luminous height is lower than DRA. The parent bodies of these two meteor showers with similar orbits will be distinct.

3.2.7 Quadrantids and December alpha Draconids

Some meteor showers appear in Draco and its neighborhood from late November to early January. These meteor showers' radiant area and appearance duration are overwrapped. First, let us start with the identification of individual meteor showers.

The radiant distribution in the target area is shown in Figure 18 divided into small (left) and large (right) semi major axis. From (a) to (h) on the left side are $1/a > 0.2$ AU and include mainly Jupiter family meteors. From (i) to (p) on the right side are $1/a < 0.2$ that include mainly Halley type or long period meteors. December alpha Draconids (#334 DAD) can be identified in $1/a > 0.2$ from 230° solar longitude (Figure 18b). December kappa Draconids (#336 DKD) can be identified in $1/a < 0.2$ from 245° (Figure 18k) to 260° (Figure 18l) solar longitude. DAD and DKD radiant areas overlap but can be separated easily by their orbit size difference thus we can identify them as independent meteor showers. Quadrantids (#10 QUA) can be identified strongly from 280 to 290° solar longitude (Figure 18g). Their radiant position is very close to DAD, and therefore Figure 19(a) plots $\lambda - \lambda_\odot$. We can find a sparse radiant concentration on the left side of Figure 19(a) until 270° solar longitude, which corresponds to DAD. The right side of Figure 19(a) after 270° solar longitude corresponds to QUA. This figure shows the gap which exists between DAD and QUA. The DAD and QUA separation can also be recognized in the perihelion longitude plot (Figure 19b). It shows that the area of radiant concentration in Figure 18(f), solar longitude 270–280°, is the initial activity of QUA by comparison with Figure 19. November lambda Draconids (#441 NLD) and November Draconids (#753 NED) are possibilities to correspond to the initial part of DAD. November i Draconids (# 392 NID) corresponds to the first half of DAD.

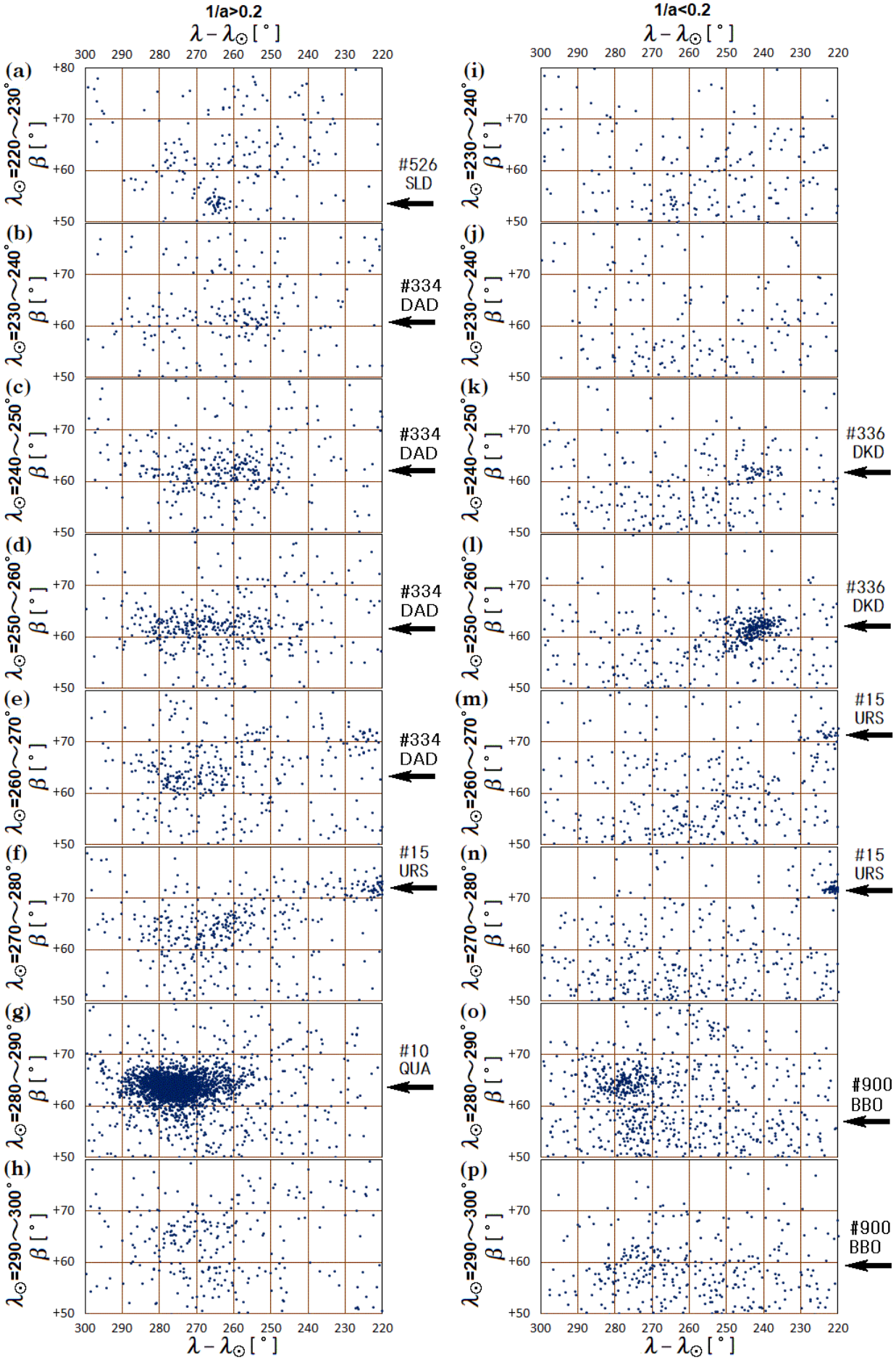

Figure 18 – Radiant area of QUA, DAD and DKD in 10° solar longitude bins. Left is short period meteors distribution and right is long period meteors.

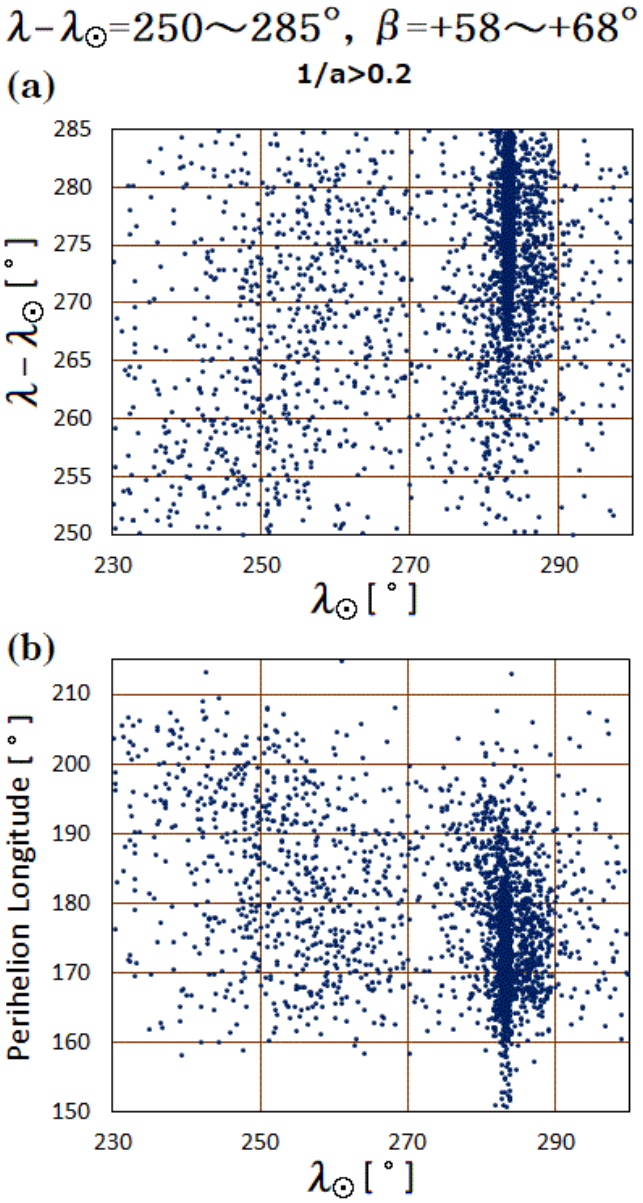

Figure 19 – DAD–QUA distinction. QUA is the denser concentration to the right of 270°.

Incidentally, in Figure 18(f), $1/a > 0.2$, $\lambda_\odot$ = 270–280°, a faint arch structure from the initial QUA radiant area to the URS radiant area is apparent. This structure, the "QUA – URS bridge", is picked up in Figure 20(a) and orbital elements are shown in Figures 20(b)–(e). The orbital element distributions in Figure 20 indicate a continuous relation between pre-QUA and URS. These meteor showers were understood to each be independent, however they might have experienced related dynamical evolution processes.

*** Quadrantids (#010 QUA)**

Double structure, namely a narrow maximum ∼1° in solar longitude accompanied by wide and weak activity (Figure 19). The weak and wide second peak turns up after a sudden decrease of the narrow main peak.

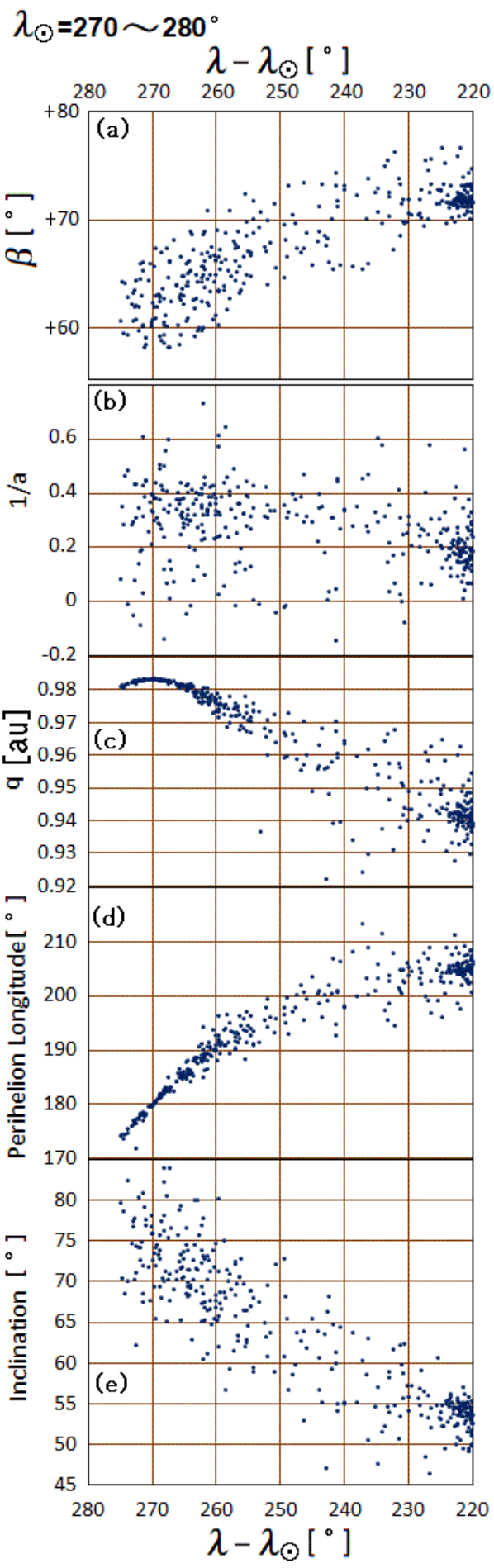

Figure 20 – Radiants and orbital elements in the "URS – QUA bridge" structure.

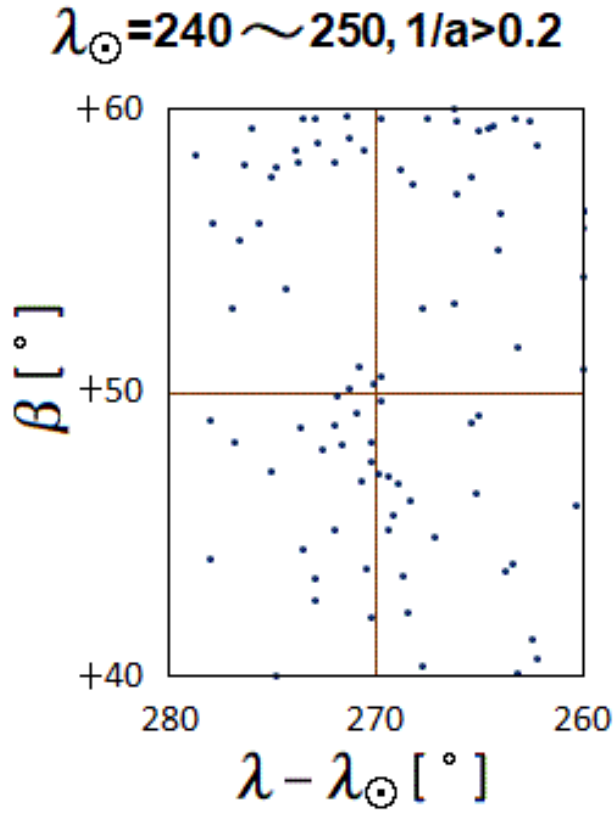

Figure 21 – GMA radiant distribution.

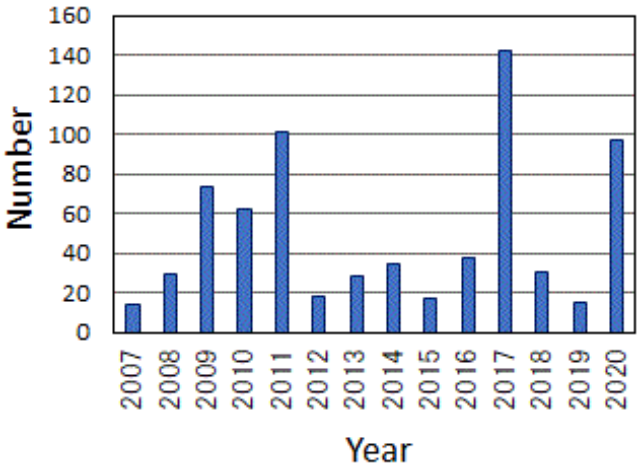

Figure 22 – Number of URS meteors in each year.

*** December alpha Draconids (#334 DAD)**

I took an additional criterion for DAD shower membership to remove $1/a < 0.2$ meteors in order to exclude meteors in the long period DKD shower.

*** gamma Ursae Majorids (#574 GMA)**

A faint meteor shower to the south of DAD radiant (Figure 21). The radiant group towards the upper part of Figure 21 belongs to DAD.

*** Ursids (#15 URS)**

Halley Type meteor shower. Very sharp maximum 1° wide in solar longitude with a superposed faint and wide component. Indistinct four year cycle of increased activity (Figure 22) demonstrates a cause related to having a constant activity peak within a narrow interval of solar longitude. That is, the Earth returns to approximately the same position on a four year cycle caused by the fractional day part of the Earth's orbital period around the Sun.

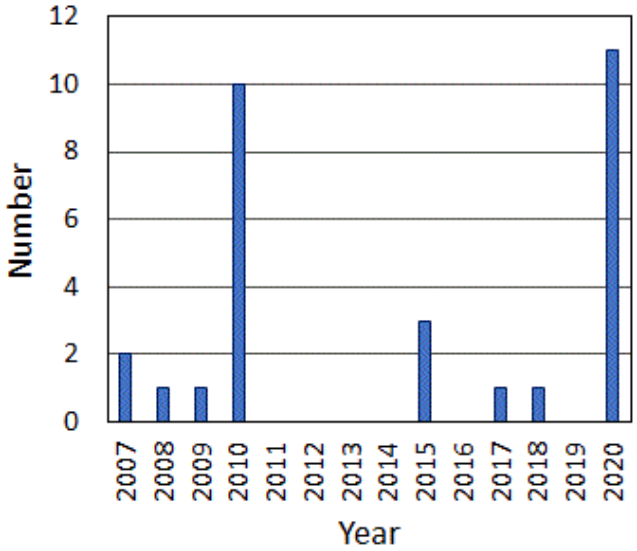

Figure 23 – Number of CCY meteors in each year.

*** gamma Ursae Minorids (#404 GUM)**

GUM orbital elements are generally similar to URS although not so similar in semi major axis and ascending node.

3.2.8 kappa Cygnids and August Draconids

Some meteor showers with similar characteristics emerge around Cygnus from the Perseid season to September. Especially, the beginning part of KCG and AUD activity are difficult to identify (Shiba, 2017).

*** kappa Cygnids (#012 KCG)**

A seven year cycle of activity is indicated because of the 5:3 resonance with Jupiter (Shiba, 2017). Thus, KCG meteors are selected only from 2007 and 2014 observations. The distribution of radiant points indicates an elongated shape north to south. Weak activity was also observed in 2013 when the radiant distribution was about 5° shifted to the north. Kappa Lyrids (#464 KLY) correspond to the early part of KCG and mu Lyrids (#413 MUL) also possibly correspond to KCG beginning activity. However, that duration is in the rainy season in Japan, so we have not got enough data.

*** chi Cygnids (#757 CCY)**

The observed variation in meteor numbers by year is indicated in Figure 23. A five year cycle of enhanced activity exists, in 2010, 2015 and 2020. The cyclic activity was pointed out by Uehara (2020) in the SonotaCo network. This cyclic activity was considered to be caused by the 7:3 resonance with Jupiter's orbital period. The distribution of radiant points shows a similar characteristic to KCG, elongated south to north. On the other hand, luminous heights have a trend to be clearly lower than KCG, implying meteoroids made of less fragile material.

*** August Draconids (#197 AUD)**

Selection of AUD meteors excluded observations of 2007 and 2014 to prevent contamination from Cygnid meteors. Figure 24 shows the variation in the AUD radiant region and its vicinity. The radiant concentration region moves to the west along a path in the shape of half an ellipse, so radiant drift cannot be described by the linear approximation equations. Moreover, the radiant distribution shape extends in the direction of the drift. August mu Draconids (#470 AMD), iota Draconids (#703 IOD) and nu Draconids (#220 NDR) correspond to parts of AUD with this unique radiant characteristic.

*** epsilon Ursae Minorids (#1044 EPU)**

Prominent activity was observed only in 2019 and over a short duration, 2° in solar longitude. Orbit shape is similar to CCY but with a difference in the orbital axis direction. Luminous height is especially low.

3.2.9 Biela Group

The shower originating from Comet 3D/Biela displayed great meteor storms in the 19th century. Now, the parent comet is thought already disintegrated, so meteor shower activity is generally faint. Radiant points drift to the north (Figure 25) as the solar longitude varies over the long duration from late October to early December. A wide radiant area structure consisted of triple components. That was constructed from some short periods active in a specific year, annual general components and near sporadic diffuse components.

*** Andromedids (#018 AND)**

I selected AND meteors from the radiant distribution figure that excluded the boundary region near sporadic meteors. Collected meteors include some small size concentrations in radiant position, distributed over time. November nu Arietids (#249 NAR) and iota Arietids (#484 IOA: removed from IAU MDC) are maybe a part of AND.

*** December phi Cassiopeiids (#446 DPC)**

Table 2 data are collected from the 2011 outburst.

3.2.10 June meteor showers

Some similar orbit faint meteor showers are observed in June. It is difficult to identify individual meteors that belong to any meteor shower. Additionally, observable meteor numbers were few because of the rainy season in Japan.

*** May psi Scorpiids (#456 MPS)**

Its activity duration is long but it is a very faint meteor shower. Xi Scorpiids (#920 XSC) is a high possibility as the beginning part of this shower. Lambda Ophiuchids (#460 LOP) may correspond to the later half of this shower. In between MPS and LOP meteor shower activity is continuous so that they seem to be the same single meteor shower. Orbit perihelion distance and inclination increase linearly as solar longitude increases. Perihelion longitude is constant around 335–336°. About 5° south of MPS, a sparse radiant distribution exists from 35 to 55° in solar longitude, with perihelion distance about half of MPS. It seems to be the April chi Librids (#140 XLI) but this is not tabulated in Table 2 because meteor numbers are few. Phi Ophiuchids (#809 USG) may be same as #140 XLI.

*** tau Herculids (#61 TAH)**

Very faint meteor shower. Orbit is similar to June Bootids (#170 JBO) indicating JBO may be one stream belonging to TAH. Epsilon Ursae Majorids (#186 EUM) may also be a member of this group.

*** June Bootids (#170 JBO)**

A definite outburst was only in 2010 (Tsuchiya et al., 2017). The prominent concentrated radiant with short activity duration indicates collision with a dense part of the stream.

*** June epsilon Ophiuchids (#459 JEO)**

A definite outburst was only in 2019. The prominent concentrated radiant with short activity duration indicates collision with a dense part of the stream.

3.2.11 Phoenicids (#254 PHO)

A definite outburst was only in 2014 (Sato et al., 2017). The November Cetids (#799 NEC) orbit is similar to PHO but with slower geocentric velocity.

3.2.12 xi Coronae Borealids (#323 XCB)

Activity characteristics vary in individual years. 2010 had high concentrated radiant distribution, 2014 radiant tended to be 3–4° further south, 2017 and 2020 had sparse radiant distribution, in other years meteor shower activity was questionable.

3.2.13 omicron Eridanids and lambda Canis Majorids

These two meteor showers and additionally December delta Eridanids (#490 DGE) and Daytime delta Triangulids (#354 DDT) may be related via their origin or evolution.

*** omicron Eridanids (#338 OER)**

The meteor shower certainly exists even with a sparse radiant distribution. The radiant position is about 15° south of the southern Taurids. Variations in orbital features are different before and after ∼253° solar longitude (Figure 26). Decreasing geocentric velocity and a somewhat increasing orbital inclination are shown till 253°. But after 253°, constant geocentric velocity and enhanced increasing inclination are shown. December delta Eridanids (#490 DGE) is estimated to correspond to OER after 253°. Daytime delta Triangulids (#354 DDT) may be a twin shower of OER because the argument of perihelion is near 90°.

*** lambda Canis Majorids (#709 LCM)**

Simultaneously with the #338 OER transition to #490 DGE, LCM appears bifurcated towards the south (Figure 27). OER can be found on the upper right side of Figure 27(a). Radiant drift characteristics resemble kappa Cygnids or chi Cygnids.

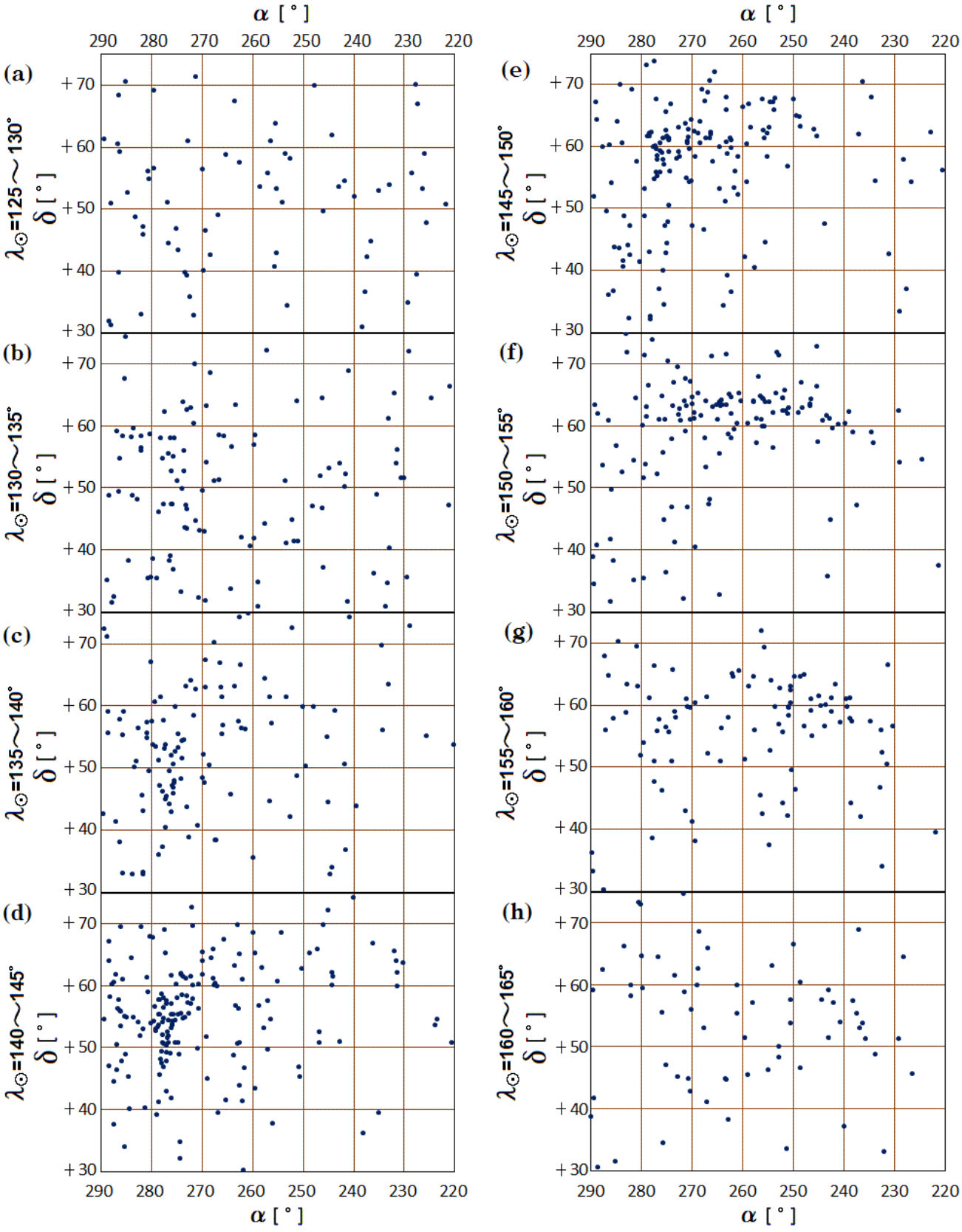

Figure 24 – Variation with solar longitude of radiant distribution in AUD area.

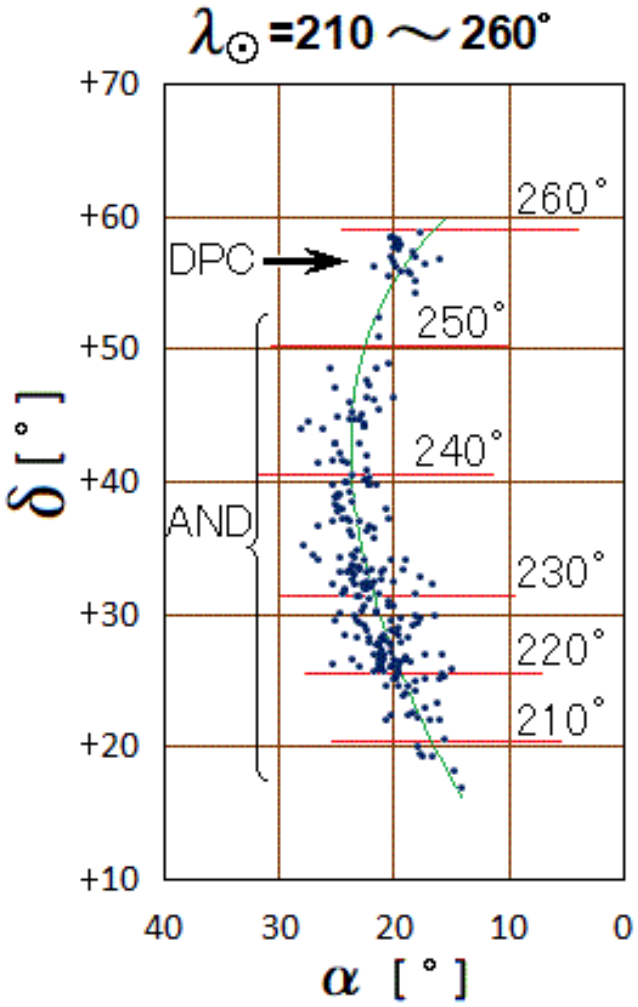

Figure 25 – Radiant distribution of AND and DPC.

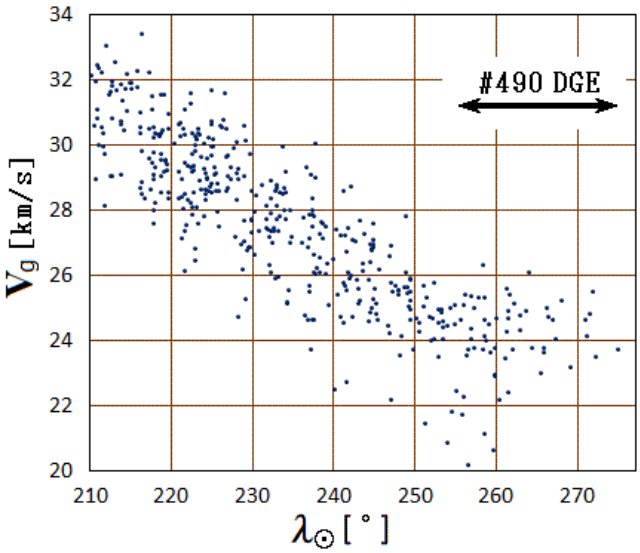

Figure 26 – Geocentric velocity of OER.

3.2.14 January xi Ursae Majorids (#341 XUM)

It is a short period meteor shower and not close to Jupiter's orbit.

3.2.15 x Herculids (#346 XHE)

Definite active years are only 2015 and 2018.

3.2.16 Southern lambda Draconids (#526 SLD)

This faint meteor shower with a compact radiant area has a high luminous altitude that indicates easy to disintegrate meteoroids.

3.2.17 e Velids (#746 EVE)

The radiant position is low in the southern sky at under 20° elevation angle but there is an annual observable meteor shower. Zeta Puppids (#300 ZPU), gamma Puppids (#301 PUP) and b Puppids (#302 PVE) are possibly the corresponding meteor shower but have slower velocity and lack some necessary orbital data. The EVE orbit is just the mirror position of DAD (#334) in the ecliptic plane.

3.2.18 Corvids (#63 COR)

I could not find any meteor shower at the IAU MDC recorded position. Especially slower velocity meteor showers are sometimes elusive for finding a radiant concentration because of too sparse a radiant distribution.

3.2.19 pi Puppids (#137 PPU)

The radiant point is on the southern sky too low to observe from Japanese latitudes.

3.2.20 October Capricornids (#233 OCC)

This meteor shower (Stream No. 53 in Terentjeva, 1989) could not be confirmed. If the geocentric velocity is in fact closer to 10.0 km/s, in accord with the 3rd entry for OCC newly added to IAU MDC citing IMO, rather than the 15.3 km/s listed by Terentjeva, then it may be possible to identify this shower in the future. The SonotaCo orbit data suggest agreement with the lower velocity although the number of meteors is not enough to draw statistically useful conclusions at this stage.

4 Discussion

SonotaCo Network observations have been used to study meteor showers whose orbital period is shorter than Jupiter's and which are close to Jupiter's orbit. This leads to data and elements on 56 meteor showers being provided (Table 2). Most of these data agree with previous research (Jenniskens et al., 2016a,b,c). However, favorable data could not be obtained for some of them. The causes of this are considerable. One is the radiant position being too low from Japanese latitudes at night time (#137 PPU). #233 OCC is doubtful by TV observation as an annual meteor shower. #63 COR maybe has concentrated orbits but is a meteor shower without a strong convergence in radiant points. Some estimated Jupiter family meteor shower results had orbital periods over 12 years which may instead be Halley type meteor showers (#183 PAU, #187 PCA, #319 JLE, #530 ECV, #569 OHY) and are excluded from Table 2. However, a few Halley type meteor showers (#320 OSE, #15 URS, #323 XCB) are included in Table 2 because they are considered related to Jupiter family meteor showers.

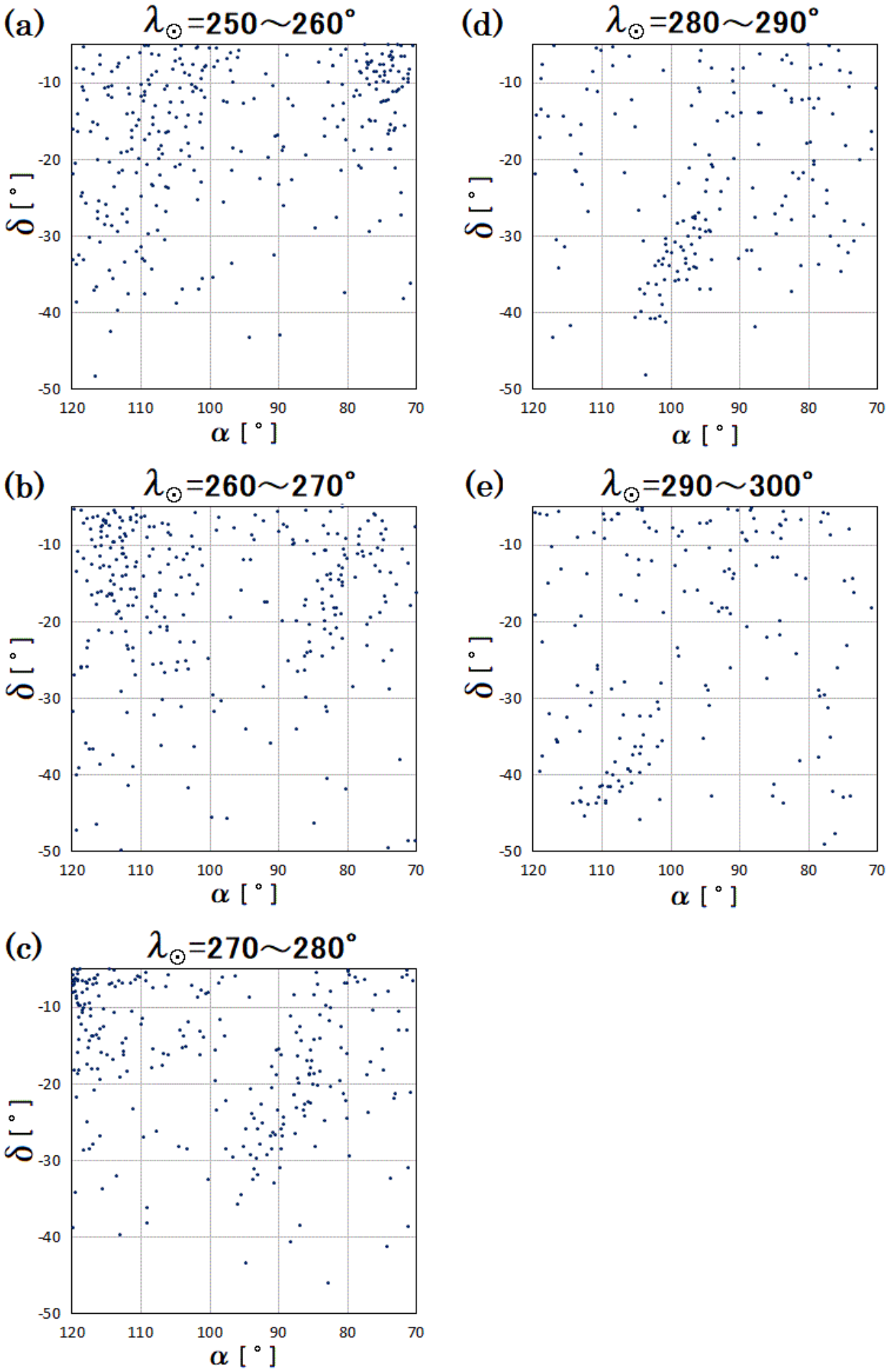

Figure 27 – Radiant distribution of LCM.

Table 3 – Meteor shower comparison: this work vs. IAU MDC.

This work			IAU MDC				
#	Code	Meteor shower name	Synonym	Pre-Shower	Post-Shower	Skewed orbital elements vary	Sub-meteor shower
1	**CAP**	alpha Capricornids	#623 XCS		#692 EQA		
2	**STA**	Southern Taurids (annual)	#626 LCT, #628 STS, #637 FTR, #625 LTA, #286 FTA				#216 SPI, #627 NPS, #28 SOA, #624 XAR
257	**ORS**	Southern chi Orionids	#636 MTA , #638 DZT				
33	**NIA**	Northern iota Aquariids	#215 NPI				
17	**NTA**	Northern Taurids	#25 NOA, #631 DAT, #630 TAR, #632 NET, #635 ATU, #629 ATS, #633 PTS, #634 TAT		#1179 OGE		
256	ORN	Northern chi Orionids	#726 DEG				
11	**EVI**	eta Virginids	#123 NVI				
21	**AVB**	alpha Virginids		#136 SLE			
47	DLI	mu Virginids	#139 GLI?		#920 XSC, #149 NOP		
150	SOP	Southern May Ophiuchids		#826 ILI			
69	**SSG**	Southern mu Sagittariids	#168 SSS	#150 SOP			
164	**NZC**	Northern June Aquilids	#1111 AQI				
165	**SZC**	Southern June Aquilids	#370 MIC				
5	**SDA**	Southern delta Aquariids	#640 AOA				#505 AIC
505	AIC	August omicron Aquariids	#642 PCE	#640 AOA			
388	**CTA**	chi Taurids					#237 SSA, #538 FFA
253	CMI	December Canis Minorids	#610 SGM		#1125 FFL	#515 OLE	
644	JLL	January lambda Leonids	#747 JKL, #710 IOL, #748 JTL				#641 DRG
171	**ARI**	Daytime Arietids			#680 JEA		
172	**ZPE**	Daytime zeta Perseids		#154 DEA			
320	**OSE**	omega Serpentids	#330 **SSE**				
334	**DAD**	December alpha Draconids	#753 NED, #441 NLD, #392 NID				
12	**KCG**	kappa Cygnids	#464 KLY	#413 MUL			
197	**AUD**	August Draconids	#470 AMD, #703 IOD, #220 NDR				
18	**AND**	Andromedids			#446 **DPC**		#249 NAR
456	MPS	May psi Scorpiids	#920 XSC, #460 LOP				#149 NOP
61	**TAH**	tau Herculids					#170 **JBO**, #186 EUM
338	**OER**	omicron Eridanids				#490 DGE	#709 LCM
746	EVE	gamma Puppids	#300 ZPU, #301 PUP, #302 PVE				

Some of this study's results are different from previous research (Jenniskens 2016a,b,c). The reason would be the different identification method of meteor showers. This study took radiant and geocentric velocity concentration but Jenniskens (2016a,b,c) adopted the "D criterion" of meteor orbit similarity, moreover applying a higher threshold than previous research. If one takes radiant and velocity concentrations for meteor shower identification, it is difficult for slow velocity meteor showers that generate wide radiant distributions (#61 TAH, #63 COR). On the other hand, a meteor shower that is sparse in terms of orbit distribution but shows more prominent characteristics in radiant concentration (#253 CMI) is easy to find in the way used by this study. Many independent meteor showers in this study are coincident with two or more meteor showers in Jenniskens (2016a,b,c), which is caused by taking a higher threshold D criterion. The meteor shower name contrasts between this study's results and the IAU MDC (Rudawska & Jopek, 2019) descriptions are shown in Table 3. The "established meteor showers" at the IAU MDC are indicated in bold in Table 3. "Synonym" in Table 3 indicates the possible same meteor showers at the IAU MDC as this study's results. In this study I took the minimum numbered meteor shower name from the IAU MDC out of multiple "synonyms" for the same meteor shower. However, #644 JLL and #330 SSE were not taken as the minimum numbered meteor showers, because the corresponding showers, #641 DRG and #320 OSE, exist only on the edge part of the active duration. "Pre-Shower" and "Post-Shower" in Table 3 are possibly the same meteor shower but there clearly exists an interruption or decrease between both meteor activities. "Skewed orbital elements vary" in Table 3 denotes that the trend in orbital elements does not vary continuously within the active time. "Sub-meteor shower" in Table 3 indicates cases where there are a few differences but similar orbital elements that possibly have the same original parent body. #002 STA (annual) consists of many "sub-meteor showers", that is to say the "Taurid complex" (Figure 3).

Generally, if many random nomenclatures apply to one object, we may be embroiled in confusing scientific discussion. To avoid this, it is better to take one name for one scientific object. On the other hand, various expressions based on multiple research paths are possible when contributing to scientific progress. From this viewpoint, permitting many nomenclatures even for one scientific object is favorable. What is the better solution to the conflicting problem?

The primary reason for the differences between this study and IAU MDC data (Table 3) is thought to be the meteor shower identification method. In this study, I defined a meteor shower when the radiant distribution on the celestial sphere showed continuous activity within the precision limit of small TV camera observations. Some calculation methods using a D criterion indicator of orbit similarity have been applied recently and been helpful for identifying meteor showers. Thus, we can judge cases where the D criterion threshold is exceeded to imply other independent meteor showers. This way is good at rejecting personal conception and making an objective judgment. The original D criterion (Southworth & Hawkins, 1963) takes the threshold based on the traditional meteor shower concept that includes the radiant distribution continuously drifting over the long term. Taking the "high threshold" method in the "D criterion" meteor shower identification technique succeeded in identifying many new showers (Jenniskens et al., 2016c). However, we must notice that if taking an arbitrary small threshold value for the D criterion, it is possible to identify a fictional new meteor shower. How to define the term "meteor shower" is necessary to continue the discussion. The classical manner, based on visual observations, required meteors conspicuously concentrated within a short duration from an identified radiant to define a "meteor shower". When photographic and TV observations became mainstream, they allowed an affinity with the D criterion to measure similarity of meteor orbits. It is a superior technique to contribute to science which has a quantitative and objective process. However, the "meteor shower" concept must contain a time axis assessment, not only a spatial axis assessment, to judge orbits' similarity. Thus, the "meteor shower" definition must contain the evolution assessment, that is, from meteoroids generated by parent objects until their end when they impact the Earth. However, we do not currently have the observation and dynamical astronomy techniques at a sufficient level to be true to the purpose of this definition. Still, I think a better way to approach its purpose is to pay attention to meteor activity continuity more than to focus on meteor orbit differences. That reason is that continuity may relate to the meteor parent body or the evolution more deeply. After this, I think that we need to contrive new evaluation criteria to judge the continuity of meteor activity objectively and quantitatively. I hope future observations make clear whether the "synonyms" in Table 3 are valid or not.

Recent progress in meteor observation techniques (Brown et al., 2008; SonotaCo, 2009; Jenniskens et al., 2016a,b,c) has contributed great numbers of meteor showers to the IAU MDC list. I should offer additional new registration procedures for the era of abundant meteor shower data. I wish to propose an IAU MDC registration standard at a qualitative level as described below. With a request to register a shower on the working list, a researcher should demonstrate fulfilling (a), (b) and (c) below. Before registering on the established list, the requirement (d) should also be fulfilled. Additionally, (a), (b) and (c) should be approved among most researchers. The first requirement (a) of four was already proposed in detail by Koseki (2016) and I recognize the progress in the improvement of the database.

(a) Enough scientific observation data

* Observer, reporter, observational method, observation site, date, time, orbital elements or radiant position with velocity and other useful data are indicated.

* Historical records or records involving unexpected observations are allowed some data to be lacking.

(b) Existence attestation of the meteor shower

* Proving or concluding orbit concentration in the solar system or concentration in radiant position with geocentric velocity.

(c) Independence attestation of the meteor shower

* Reported new meteor shower exists nearby no previous meteor showers or a gap exists between already known and new meteor shower and/or both showers' origin and evolution differences are indicated.

(d) Objectivity attestation

* Two or more independent teams' reports are published containing (a), (b) and (c), that agree with each other subject to the individual errors.

Finally, five meteor showers were labeled "periodic" in the "Activity" column of Table 2. Meteor showers characterized by periodic activity, caused by resonance with Jupiter, need to be described differently against "annual" meteor showers. I advise adding "periodic" or "resonance" as an option in the "Activity" classification, further to the present options "annual" and observed year(s) at the IAU MDC.

Acknowledgements

This study is based on the SonotaCo network members' database that contributes daily to taking meteor images and analyzing them. This study depends on these SonotaCo network members. I say thank you to them for their long term contributions. Mr. SonotaCo manages this network and moreover, has offered superior software for the analysis. Mr. Mikiya Sato and Dr. Koji Maeda gave me valuable comments about various meteor showers.

References

Asher D. J. and Izumi K. (1998). "Meteor observations in Japan: new implications for a Taurid meteoroid swarm". *Mon. Not. Roy. Astron. Soc.*, **297**, 23–27.

Brown P., Weryk R. J., Wong D. K., and Jones J. (2008). "A meteoroid stream survey using the Canadian Meteor Orbit Radar. I. Methodology and radiant catalogue". *Icarus*, **195**, 317–339.

Drummond J. D. (1981). "A test of comet and meteor shower associations". *Icarus*, **45**, 545–553.

Jenniskens P., Jopek T. J., Janches D., Hajduková M., Kokhirova G. I., and Rudawska R. (2020). "On removing showers from the IAU working list of meteor showers". *Planet. Space Sci.*, **182**, 104821.

Jenniskens P., Nénon Q., Albers J., Gural P. S., Haberman B., Holman D., Morales R., Grigsby B. J., Samuels D., and Johannink C. (2016a). "The established meteor showers as observed by CAMS". *Icarus*, **266**, 331–354.

Jenniskens P., Nénon Q., Gural P. S., Albers J., Haberman B., Johnson B., Holman D., Morales R., Grigsby B. J., Samuels D., and Johannink C. (2016b). "CAMS confirmation of previously reported meteor showers". *Icarus*, **266**, 355–370.

Jenniskens P., Nénon Q., Gural P. S., Albers J., Haberman B., Johnson B., Morales R., Grigsby B. J., Samuels D., and Johannink C. (2016c). "CAMS newly detected meteor showers and the sporadic background". *Icarus*, **266**, 384–409.

Jopek T. J. and Jenniskens P. M. (2011). "The Working Group on Meteor Shower Nomenclature: a history, current status and a call for contributions". In Cooke W. J., Moser D. E., Hardin B. F., and Janches D., editors, *Meteoroids: The Smallest Solar System Bodies, Proceedings of the Meteoroids Conference held in Breckenridge, Colorado, USA, May 24-28, 2010*. NASA/CP-2011-216469, pages 7–13.

Jopek T. J. and Kaňuchová Z. (2014). "Current status of the IAU MDC meteor showers database". In Jopek T. J., Rietmeijer F. J. M., Watanabe J., and Williams I. P., editors, *Meteoroids 2013, Proceedings of the International Conference held at the Adam Mickiewicz University, Poznań, Poland, Aug. 26-30, 2013*. A. M. Univ. Press, pages 353–364.

Jopek T. J. and Kaňuchová Z. (2017). "IAU Meteor Data Center–the shower database: A status report". *Planet. Space Sci.*, **143**, 3–6.

Koseki M. (2016). "Research on the IAU meteor shower database". *WGN, Journal of the IMO*, **44:5**, 151–169.

Neslušan L., Porubčan V., Svoreň J., and Jakubík M. (2020). "On the new design of the IAU MDC portal". *WGN, Journal of the IMO*, **48:6**, 168–169.

Rudawska R. and Jopek T. J. (2019). "IAU Meteor Data Center". `http://www.ta3.sk/IAUC22DB/MDC2007` .

Sato M., Watanabe J., Tsuchiya C., Moorhead A. V., Moser D. E., Brown P. G., and Cooke W. J. (2017). "Detection of the Phoenicids meteor shower in 2014". *Planet. Space Sci.*, **143**, 132–137.

Sekanina Z. (1973). "Statistical model of meteor streams. III. Stream search among 19303 radio meteors". *Icarus*, **18**, 253–284.

Shiba Y. (2016). "Taurid swarm exists only in southern branch (STA)". *WGN, Journal of the IMO*, **44:3**, 78–91.

Shiba Y. (2017). "Kappa Cygnids (KCG) by TV observation results". *WGN, Journal of the IMO*, **45:6**, 127–143.

Shiba Y. (2018). "Eta Virginids (EVI) four year cycle". *WGN, Journal of the IMO*, **46:6**, 184–190.

SonotaCo (2009). "A meteor shower catalog based on video observations in 2007–2008". *WGN, Journal of the IMO*, **37:2**, 55–62. (see also "SonotaCo Network Simultaneously Observed Meteor Data Sets", `http://sonotaco.jp/doc/SNM/`).

Southworth R. B. and Hawkins G. S. (1963). "Statistics of meteor streams". *Smithson. Contrib. Astrophys.*, **7**, 261–285.

Terentjeva A. K. (1989). "Fireball streams". *WGN, Journal of the IMO*, **17:6**, 242–245.

Tsuchiya C., Sato M., Watanabe J., Moorhead A. V., Moser D. E., Brown P. G., and Cooke W. J. (2017). "Correction effect to the dispersion of radiant point in case of low velocity meteor showers". *Planet. Space Sci.*, **143**, 142–146.

Ueda M. (2019). "Observational guide". *Astronomical Circular, Nippon Meteor Society*, **924**, 2–7. (In Japanese).

Uehara S. (2020). "CCY (Chi-Cygnids) appears for the first time in 5 years". `http://sonotaco.jp/forum/viewtopic.php?t=4676` . (In Japanese).

Handling Editor: David Asher

The role of meteoric influx and the geomagnetic disturbance on the seasonal forming of sporadic E over Europe

Wolfgang Kaufmann[1]

The seasonal forming of a sporadic E (Es) layer over Europe was analysed by Es layer critical frequency data from six European ionosondes, the planetary Ap-Index and radio meteor echo counts from three European stations. The influence of seasonal varying meteoric influx and geomagnetic disturbance of Earth's magnetic field on the seasonal forming of the Es layer was found to be ambivalent. The occurrence of a high electron density Es layer coincided remarkably with the level of the combined number of counted meteors and geomagnetic Ap Index from February to September whereas this was not true for the remaining months.

Received 2022 March 2

1 Introduction

A sporadic E (Es) layer is a thin highly ionised temporary layer in the atmosphere at about 100 km height. According to the widely accepted Windshear Theory (Whitehead, 1961; Axford, 1963; Whitehead, 1997) the central forces of the forming process of a sporadic E layer are the Earth's magnetic field, the atmospheric metallic ion concentration and wind shears in horizontal neutral winds in the mesosphere/lower thermosphere, MLT (for a comprehensive review see Haldoupis, 2011). The evolving of a thin layer of compressed positively charged metallic ions between two stacked reverse wind flows by geomagnetic Lorentz forcing is followed by the attraction of free electrons moving along the magnetic field lines to neutralize this charge. The resulting clouds with a high density of free electrons represent the Es layer and are responsible for the refraction of radio waves. Solar driven oscillations of the wind flows in the MLT modulate the diurnal forming of Es in a characteristic manner that can be observed even by means of an amateur (Kaufmann, 2021). Furthermore, the mid-latitude forming of Es shows a perspicuous seasonal dependence that is marked by a pronounced summer maximum.

Haldoupis et al. (2007) suggested that the seasonal sporadic E layer forming is determined by the supply of the atmosphere with metallic ions originating from incoming ablating meteoroids. However, e.g. Mubasshir Shaikh et al. (2021) denied such correlation over the Arabian peninsula. No clear picture can be gained from literature about the influence of the meteoric influx on Es forming. Hence, the aim of this study is to analyse the situation in Europe. Forward scattered radio waves off ionised meteor trails were employed as an estimate of the influx of meteors over Europe. These data were

[1]Lindenweg 1e, 31191 Algermissen, Germany. Email: contact@ars-electromagnetica.de

IMO bibcode WGN-502-kaufmann-sporadice
NASA-ADS bibcode 2022JIMO...50...62K

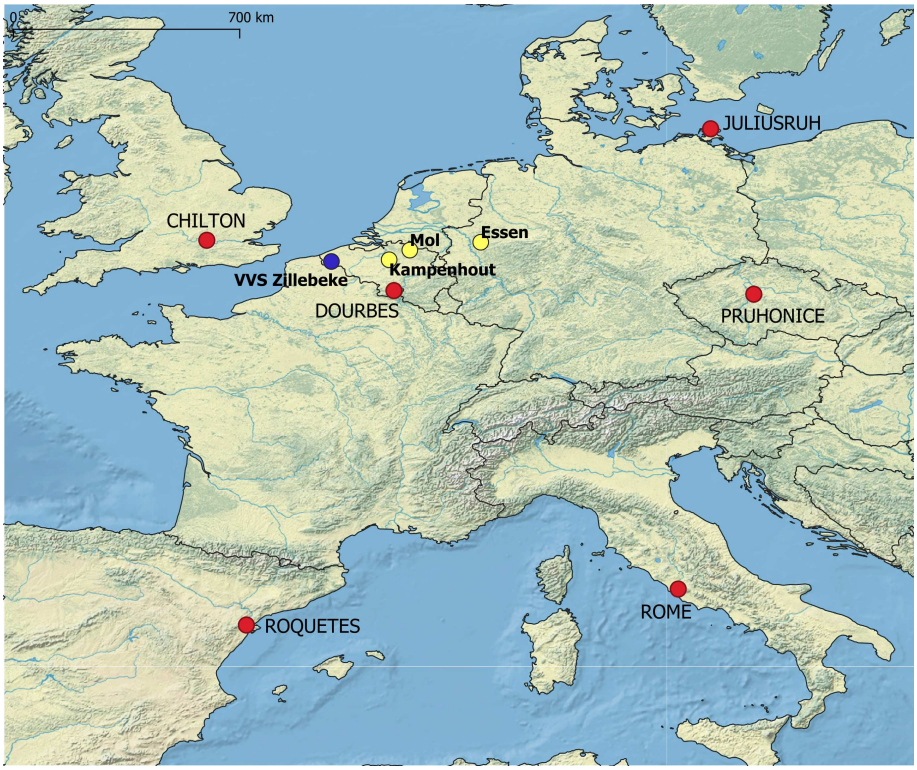

Figure 1 – Positions of the six Ionosondes (red), the three radio observation stations (yellow) and the applied transmitter (blue). Map made with Natural Earth.

taken from three receiving radio stations using the same continuously transmitting radio frequency beacon. This gives most homogenous data-sets.

The occurrence of Es was derived from daily Es layer critical frequency (fo Es) of 6 different European ionosondes. Thereby, the level of the frequency directly depends on the concentration of free electrons in the Es layer. A one year time series of the fo Es was considered together with the corresponding daily count rates of radio meteors. Additionally the daily geomagnetic Ap-Index was included in the analysis as a suspected influencing factor of Es-forming.

2 Data and Methods

The analysis was performed for the time period 2020-01-01 to 2020-12-31. The radio observed number of daily meteors were provided by F. Verbelen, Kampenhout, C. Steyaert, Mol and WHS, Essen. They employed the VVS-beacon at Zillebeke as transmitter at 49.99 MHz. From the European ionosondes Chilton, Juliusruh, Pruhonice, Dourbes, Roquetes and Rome data about Es layer critical frequency (fo Es) were retrieved from the Lowell GIRO Data Center (LGDC)[a]. The ionosondes were picked approximately on a circle around these meteor measuring stations or being directly adjacent, respectively, see Figure 1. The planetary Ap-Indices were downloaded from the GFZ German Research Centre for Geosciences[b] (Matzka et al., 2021a).

Each ionosonde performed a couple of fo Es measurements per day. For reducing them to a one day value the fo Es maximum value per day and ionosonde was taken. The maximum value was chosen to focus on the highest electron densities evolving on each day. Thereby only those measurements were taken into account that had an auto-scaling confidence score ≥ 75. The confidence score is a measure of the reliability of Es detection by the ionosonde's feature recognition algorithm. From the 8 daily 3h-Ap-Index measurements the maximum-value per day was taken. From the three radio meteor observing stations daily count rates (dCR) were derived. To each of these time series a 25-day moving average was applied. Hereby, short-term daily fluctuations were balanced out, long-term trends became visible. Subsequently the smoothed time series were normalised to 0–1. From the time series of the six ionosondes as well as of the three radio meteor observing stations a daily mean was calculated. Thus three basic measures were available: fo_{25} Es, Ap_{25} and dCR_{25}. For further smoothing at least these three time series were decomposed into seasonal, trend, and residual components by a statistical time series algorithm. From this the trend component was used whereby calculating a 10 day trend was found to be appropriate: fo_{25} Es (trend), Ap_{25} (trend) and dCR_{25} (trend).

[a] http://spase.info/SMWG/Observatory/GIRO
[b] https://www.gfz-potsdam.de/kp-index/

3 Results

Figure 2 shows the course of fo_{25} Es (trend), Ap_{25} (trend) and dCR_{25} (trend). Looking at the fo_{25} Es (trend) curve it should be pointed out, that an Es layer obviously was present throughout the year. However, its electron density only shows a pronounced summer maximum in May to August, a small local maximum in October and a second small local maximum in January. The dCR_{25} (trend) curve shows two broad maxima: one in May to August and one in October to December. Also the Ap_{25} (trend) has a seasonal shaped time course which can be observed generally: Matzka et al. (2021b) found a marked seasonal variation with equinoctial maxima analysing the period 1932–2019.

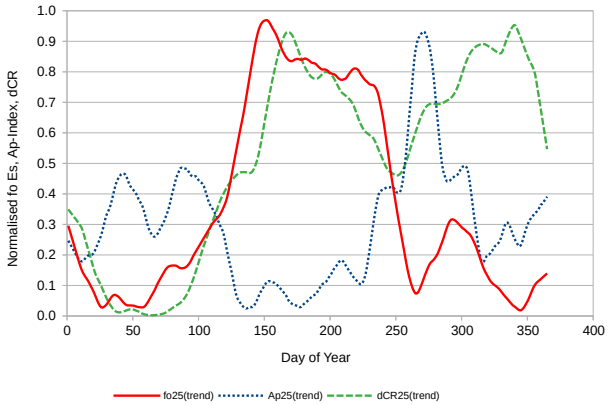

Figure 2 – The smoothed and normalised curve progression of critical frequency of the Es layer (fo_{25} Es (trend), red solid line), the meteor counts (dCR_{25} (trend), dashed green line) and planetary A-Index (Ap_{25} (trend), blue dotted line) in the year 2020.

The occurrence of the summer maxima of both the fo_{25} Es (trend) and dCR_{25} (trend) is astonishingly synchronous. The same is true for the minimum of Ap_{25} (trend). Combining dCR_{25} and Ap_{25} could lead to an even better approximation to fo_{25} Es. Therefore, a simple additive model was adopted:

$$f(Ap, dCR) = -Ap_{25}\,(trend) + dCR_{25}\,(trend)$$

The result is depicted in Figure 3. In the time period from about February-September the f(Ap, dCR) curve correlates well with the fo_{25} Es (trend) curve. The small

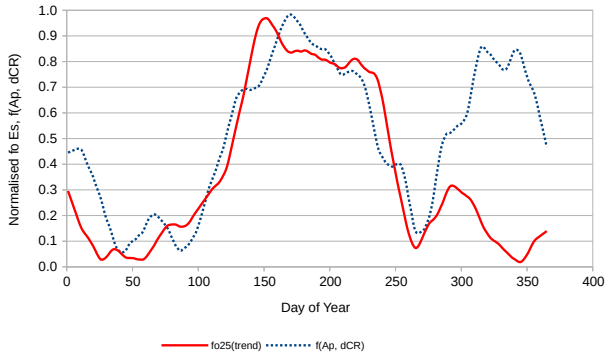

Figure 3 – The smoothed and normalised curve progression of critical frequency of the Es layer (fo_{25} Es (trend), red solid line) and combined meteor counts / Ap-Indices (f(Ap, dCR), blue dotted line) in the year 2020.

local October maximum of fo_{25} Es (trend) initially follows the f(Ap, dCR) curve. However, with increasing temporal distance from the summer the degree of correlation decreases fast. Especially in November and December both curves show the largest deviation between them.

4 Discussion

Six European ionosondes being arranged around the transmitter/receiver set provided a geographical and statistical solid base for the analysis. The normalisation of all data time series eliminated individual differences in the values of the measured data and emphasised their trends. Choosing three radio stations listening to same transmitter guaranteed a radio meteor detection area lying in between the location of the six ionosondes. Briefly, the area where radio meteors can be detected is defined by ellipsoids with the position of the receiver and the transmitter as foci and the trajectories of the meteors tangential to these ellipsoids (Rendtel & Arlt, 2015). Employing three stations not only reduced the influence of possible false positives but also enhanced the meteor detection area. Furthermore the influence of the individual transmitter – meteor-trajectory – receiver geometries on the local meteor detection-rates was relativized.

As shown in Figure 3 the additive combination of dCR_{25} and Ap_{25} was able to reproduce the course of fo_{25} Es remarkably well from February to September. To evaluate their match in more detail the difference between the time series of fo_{25} Es (trend) and f(Ap, dCR) was calculated per each day and plotted in Figure 4. The standard deviation (sd) of the calculated difference was used as a matching-criterion. The range of one sd was centred around the zero line in Figure 4. Thus the time periods could be estimated in which the difference between fo_{25} Es (trend) and f(Ap, dCR) is within the span of one sd. Using this approach an essentially continuous match was found from February to September 2020 (days 32–273, corresponding to February 1st and September 29th, respectively).

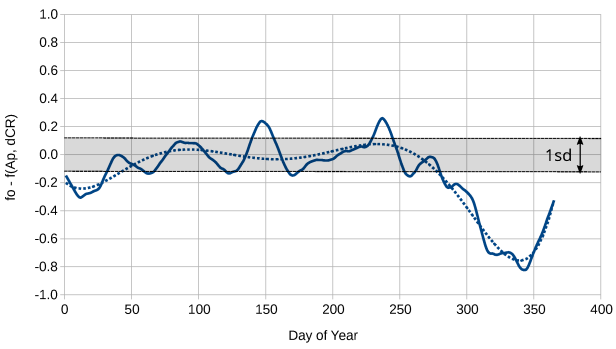

Figure 4 – Plot of the difference between fo_{25} Es and f(Ap, dCR) as shown in Figure 3. The standard deviation centred around zero and a smoothing polynomial of 6th order (dotted line) are indicated.

This result does not support any of the conflicting data in the literature. On the one hand there is a remarkable match in the temporal evolvement of the combined meteor count rates / Ap-Indices and the Es layer critical frequency from February to September. On the other hand the same factor combination is not able to explain the low electron density of the Es layer from October to January. Following, it may suggest that the seasonal variation of these two factors do not seem to play a key role in the seasonal variation of Es forming generally or at least during autumn-/winter. However, their surprising correlation with the Es occurrence during nine months of the year may assign them a modulating effect.

An explanation for the diverse findings could result from different methods used to estimate the meteoric influx. None of the used techniques (radar backscatter, forward scatter, visual) is capable to deliver a continuous 24 h observation based on a spatially uniform responsivity over the whole hemisphere. The distribution of detectable meteoroid masses also differs between the techniques and observing stations. This may strongly bias the estimate of meteoric influx.

Moreover, it should be kept in mind, that seasonal different wind regimes in the MLT could be responsible for the seasonal variation of Es layer forming. Recently, a large number of neutral wind measurements from the Ionospheric Connection Explorer (ICON) mission (Immel et al., 2018) became available, providing an opportunity for direct comparison of Es with the local wind shear.

5 Conclusion

No unequivocal information about the role of the seasonal varying meteoric influx and planetary A-Index could be gained to explain the seasonal variation of Es layer forming over Europe. The assumption that the seasonal variation of these two factors are the main drivers of the seasonal occurrence of Es could not be supported by this study. On the other hand, the influence of these two factors cannot be denied. At least their seasonal variation may have a modulating effect.

Acknowledgment

Meteor data kindly were provided by Felix Verbelen (personal communication) as well as Chris Steyaert and WHS Essen via RMOB[c]. This paper uses data from the Juliusruh Ionosonde which is owned by the Leibniz Institute of Atmospheric Physics Kuehlungsborn, from the ionospheric observatory in Dourbes, owned and operated by the Royal Meteorological Institute (RMI) of Belgium, from the Observatory of Ebre, Spain, from the Chilton ionosonde operated by the Rutherford Appleton Laboratory, from the Průhonice Observatory of the Institute of Atmospheric Physics CAS and from the Rome Observatory of the Istituto Nazionale di Geofisica e Vulcanologia. The Ap-Index is taken from the GFZ German Research Centre for Geosciences.

[c] https://www.rmob.org/index.php

References

Axford W. I. (1963). "The Formation and Vertical Movement of Dense Ionized Layers in the Ionosphere Due to Neutral Wind Shears". *Journal of Geophysical Research*, **68:3**, 769–779.

Haldoupis C. (2011). "A tutorial review on sporadic e layers". In Abdu M. A. and Pancheva D., editors, *Aeronomy of the Earth's Atmosphere and Ionosphere*, pages 381–394. Springer Science+Business Media B.V.

Haldoupis C., Pancheva D., Singer W., Meek C., and MacDougall J. (2007). "An explanation for the seasonal dependence of midlatitude sporadic E layers". *Journal of Geophysical Research (Space Physics)*, **112:A6**, A06315.

Immel T. J., England S. L., Mende S. B., Heelis R. A., Englert C. R., Edelstein J., Frey H. U., Korpela E. J., Taylor E. R., Craig W. W., Harris S. E., Bester M., Bust G. S., Crowley G., Forbes J. M., Gérard J. C., Harlander J. M., Huba J. D., Hubert B., Kamalabadi F., Makela J. J., Maute A. I., Meier R. R., Raftery C., Rochus P., Siegmund O. H. W., Stephan A. W., Swenson G. R., Frey S., Hysell D. L., Saito A., Rider K. A., and Sirk M. M. (2018). "The Ionospheric Connection Explorer Mission: Mission Goals and Design". *Space Science Reviews*, **214:1**, 1–36.

Kaufmann W. (2021). "Study of Sporadic E Occurrence in Europe 2021". *WGN, Journal of the IMO*, **49:5**, 114–119.

Matzka J., Bronkalla O., Tornow K., Elger K., and Stolle C. (2021b). "Geomagnetic Kp index. V. 1.0.". `https://doi.org/10.5880/Kp.0001` .

Matzka J., Stolle C., Yamazaki Y., Bronkalla O., and Morschhauser A. (2021a). "The Geomagnetic Kp Index and Derived Indices of Geomagnetic Activity". *Space Weather*, **19:5**, e02641.

Mubasshir Shaikh M., Gopakumar G., Abdulla Alowais A., Essa Sharif M., and Fernini I. (2021). "Contribution of meteor flux in the occurrence of sporadic-E (Es) layers over the Arabian Peninsula". *Annales Geophysicae*, **39:3**, 471–478.

Rendtel J. and Arlt R. (2015). *Handbook for Meteor Observers*. International Meteor Organization, Potsdam.

Whitehead D. (1997). "Sporadic E — A Mystery Solved? Part 2". *QST*, pages 38–42.

Whitehead J. D. (1961). "The formation of the sporadic-E layer in the temperate zones". *Journal of Atmospheric and Terrestrial Physics*, **20:1**, 49–58.

Handling Editor: Javor Kac

Preliminary results

Result of the IMO Video Meteor Network – Third Quarter 2019

Sirko Molau[1], *Stefano Crivello, Rui Goncalves, Carlos Saraiva, Enrico Stomeo, Jörg Strunk, and Javor Kac*

The IMO Video Meteor Network cameras recorded about 32 000 meteors in more than 7 700 observing hours during 2019 July, over 73 000 meteors in more than 12 000 observing hours during 2019 August, and more than 50 000 meteors in nearly 12 000 observing hours during 2019 September. Flux density profiles are presented for the α-Capricornids, July γ-Draconids, Southern δ-Aquariids, Perseids, κ-Cygnids, α-Aurigids, and September ε-Perseids.

Received 2022 April 24

1 Introduction

In the third quarter of 2019 we operated about 80 active meteor cameras in the IMO Network, similar to previous months. The weather was fine most of the time, with just short periods of poor observing conditions around July 14 and 28, and between September 7 and 9, when the number of active cameras dropped dramatically (Figure 1). Nevertheless, the output of the Network remained well below previous years. 76 active cameras in July recorded about 32 000 meteors in well over 7 700 hours of effective observing time. In August we had 82 active cameras that captured over 73 000 meteors in over 12 000 observing hours. Both were the worst monthly results since 2014. In September we operated 80 cameras. Their output was about 50 000 meteors in nearly 12 000 hours of observing time. That was still below average, but at least not the worst result since 2014.

With regards to the meteor count we can clearly see the summer peak in Figure 2. Even though the hourly average of four meteors per hour in early July is well above the annual minimum, we have short summer nights which limit the absolute number of meteors that can be recorded in the northern hemisphere. Towards the end of July, we have several active meteor showers (α-Capricornids, Southern δ-Aquariids, Perseids) and the nights are getting longer, which raises the meteor counts significantly. In mid-August we reach the annual maximum. During the Perseid peak nights we record fifteen meteors per hour and more. In September the numbers reduce again, but the average hourly rate is still twice as high as in early July.

2 Activity profiles

With all observations having been uploaded to the flux database, we can now have a look at the activity profiles of meteor showers in the third quarter of 2019. In fact, thanks to new functions in `meteorflux.org` (accessed 2022 April 24), we can derive population index profiles in parallel.

[1]Abenstalstr. 13b, 84072 Seysdorf, Germany.
Email: `sirko@molau.de`

IMO bibcode WGN-502-molau-2019q3
NASA-ADS bibcode 2022JIMO...50...66M

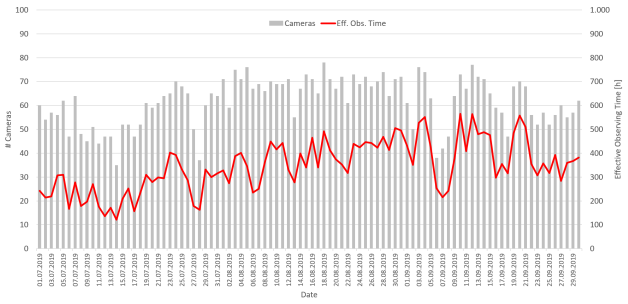

Figure 1 – Number of active cameras per night (grey bars) and effective observing time of these cameras (red line) in the third quarter of 2019.

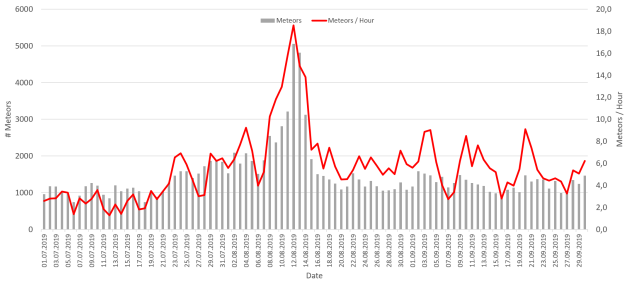

Figure 2 – Number of recorded meteors per night (grey bars) and average number of meteors per hours (red line) in the third quarter of 2019.

2.1 α-Capricornids

Let us start with the α-Capricornids. Figure 3 shows their activity profile of 2019 compared with the long-term profile of the years 2011 to 2018. We see some

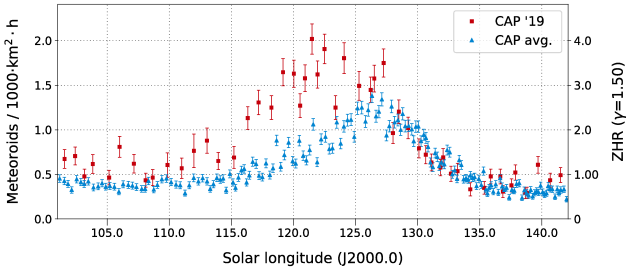

Figure 3 – Flux density of the α-Capricornids in 2019 (red squares) along with the average of the years 2011–2018 (blue triangles), derived from observations of the IMO Network.

remarkable deviations. The profile as such looks similar, but the whole activity seems to be shifted earlier by 5° solar longitude. The peak has already occurred at 122° solar longitude, in contrast to 127° solar longitude in the long-term average.

The population index of the α-Capricornids starts at values above $r = 2.5$, but we assume that sporadic pollution is dominating at the edges of the activity profile. At the activity peak the population index is $r = 2.6$, and at the descending activity branch in drops to $r = 2.3$. This behaviour fits perfectly to the long-term profile with a minimum population index of $r = 2.0$ at 129° solar longitude only shortly after the flux density peak (Figure 4).

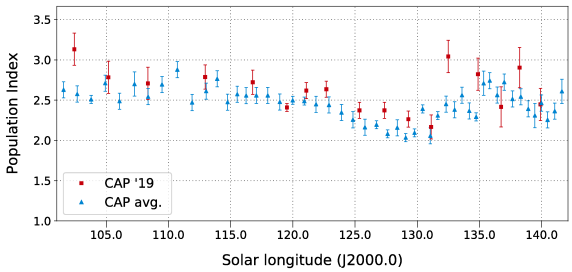

Figure 4 – Population index of the α-Capricornids in 2019 (red squares) along with the average of the years 2011–2018 (blue triangles), derived from observations of the IMO Network.

2.2 July γ-Draconids

The July γ-Draconids (Figure 5) hardly emerge from the sporadic background in 2019, similar to previous years with the exception of 2016, when they experienced a brief outburst.

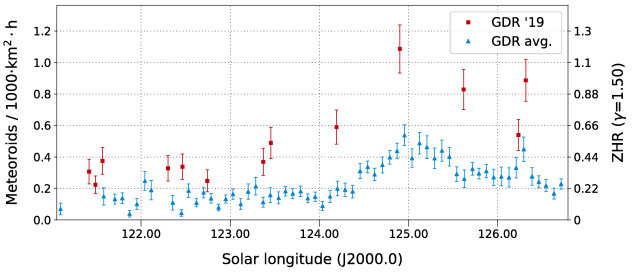

Figure 5 – Flux density of the July γ-Draconids in 2019 (red squares) along with the average of the years 2011–2018 (without 2016, blue triangles), derived from observations of the IMO Network.

2.3 Southern δ-Aquariids

In case of the Southern δ-Aquariids, the activity profile of 2019 fits nicely to the average of 2011 to 2018 (Figure 6) – but the absolute flux density value remains well below the average. Whereas we typically observe values of up to 30 meteoroids per 1 000 km^2 per hour, it was only 20 meteoroids in 2019.

According to the IMO Meteor Shower Calendar (Rendtel, 2018), the population index drops from values of $r = 3.0$ away from the peak to $r = 2.5$ at the

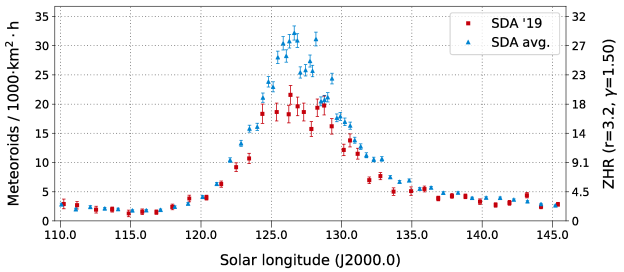

Figure 6 – Flux density of the Southern δ-Aquariids in 2019 (red squares) along with the average of the years 2011–2018 (blue triangles), derived from observations of the IMO Network.

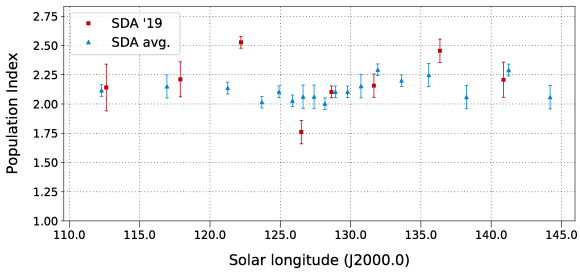

Figure 7 – Population index of the Southern δ-Aquariids in 2019 (red squares) along with the average of the years 2011–2018 (blue triangles), derived from observations of the IMO Network.

activity maximum. In the 2019 profile (Figure 7) we can see the drop clearly, but starting from $r = 2.5$ to values of $r = 1.8$. In the long-term profile the dip is less intense. Here we start with values of $r = 2.2$ before the peak. The population index falls to $r = 2.0$ during the peak, and rises to $r = 2.3$ thereafter.

2.4 Perseids

Let us now continue with the highlight of the year, the Perseids. Figure 8 compares at first the overall activity profile of 2019 with the average of the years 2011 to 2018. We notice the slow increase from mid-July to early August. At around 137° solar longitude the rate is rising dramatically, and it peaks at 139°.5 solar longitude. Thereafter the rate is declining, albeit a little slower and taking a little longer. Only from 142° solar longitude is the decrease decelerating, and a week later

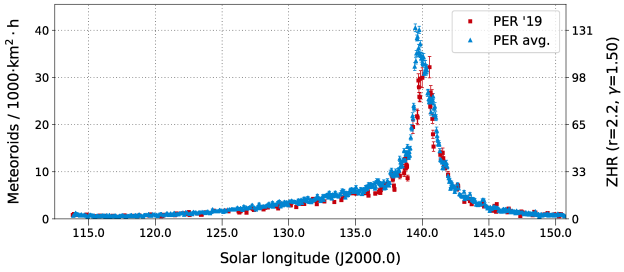

Figure 8 – Flux density of the Perseids in 2019 (red squares) along with the average of the years 2011–2018 (blue triangles), derived from observations of the IMO Network.

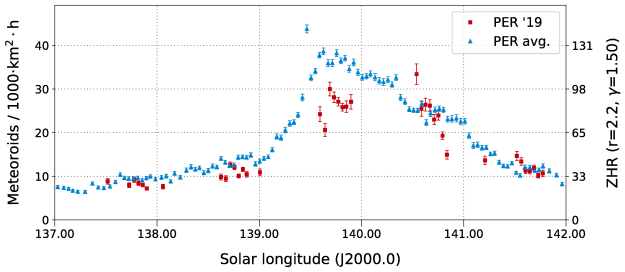

Figure 9 – Flux density of the Perseids near their peak in 2019 (red squares) along with the average of the years 2011–2018 (blue triangles), derived from observations of the IMO Network.

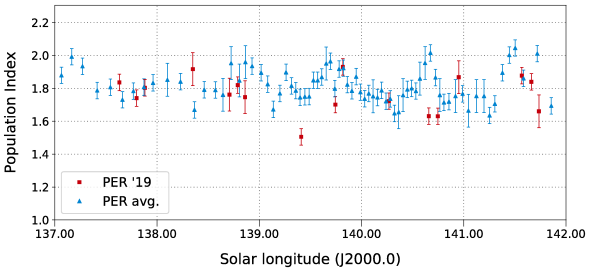

Figure 10 – Population index of the Perseids near their peak in 2019 (red squares) along with the average of the years 2011–2018 (blue triangles), derived from observations of the IMO Network.

the Perseids are lost in the sporadic background. In this respect, 2019 data fit perfectly to the long-term profile.

If we have a closer look at the peak time (Figure 9) we still have a good match. Only the peak flux density of about 30 meteoroids per 1 000 km^2 per hour in 2019 is below average.

The population index profile of the Perseids differs from that of other showers. It is nearly constant and only oscillates between values of $r = 1.7$ and $r = 2.0$. The 2019 profile fits well into that trend, but we measured a slightly smaller value just at the shower peak. Overall, the brightness distribution is nearly constant and the fraction of bright meteors quite high (Figure 10).

This behaviour does not change when we extend the graph to the full activity interval of the Perseids. Not surprisingly, the population index shows strong scatter at the edges due to sporadic pollution, but the r-values remain rather low at all times (Figure 11).

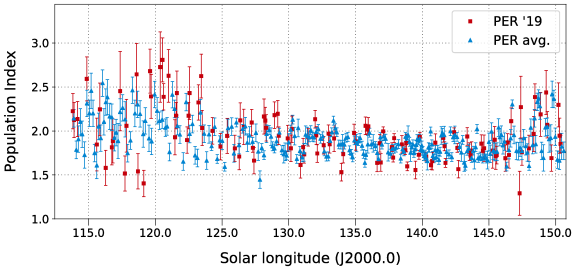

Figure 11 – Population index of the Perseids in 2019 (red squares) along with the average of the years 2011–2018 (blue triangles), derived from observations of the IMO Network.

2.5 κ-Cygnids

The κ-Cygnids are active throughout most of August. Their flux density is low, but they can still be distinguished clearly from the background. When comparing the activity profile of 2019 with the long-term average (Figure 12) we left out 2014, when the shower experienced an outburst (Rendtel & Molau, 2015). Overall, the 2019 data fit well to the long-term profile.

The population index of the κ-Cygnids is $r = 2.6$ at the edges, and it drops to values near $r = 2.2$ at the activity peak. The 2019 profile in this respect also follows the long-term trend (Figure 13). Note that the activity profile shows a kind of double-peak at 140° and 146° solar longitude. At the same time, we see dips in the population index profile. Maybe we are observing here two components of the shower.

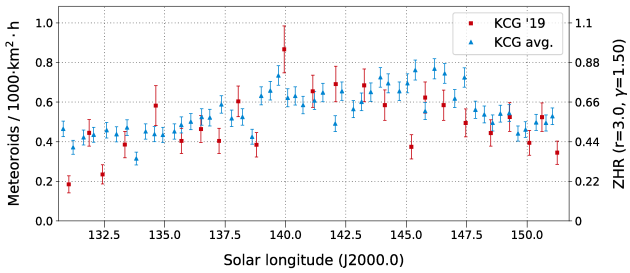

Figure 12 – Flux density of the κ-Cygnids in 2019 (red squares) along with the average of the years 2011–2018 (without 2014, blue triangles), derived from observations of the IMO Network.

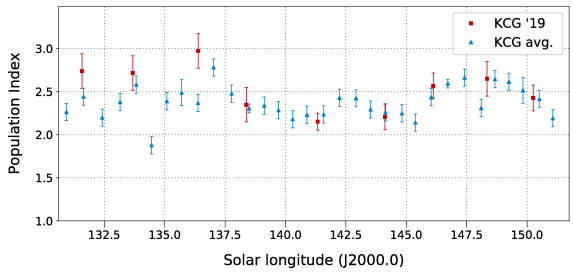

Figure 13 – Population index of the κ-Cygnids in 2019 (red squares) along with the average of the years 2011–2018 (without 2014, blue triangles), derived from observations of the IMO Network.

2.6 α-Aurigids

Finally, we want to analyse two showers of September. The α-Aurigids (Figure 14) can hardly be discerned from the sporadic background – neither in 2019 nor in the long-term activity profile.

2.7 September ε-Perseids

The September ε-Perseids present often a surprise to the observers – most recently in 2008 and 2013 (Jenniskens et al., 2008; Molau et al., 2013; Rendtel et al.,

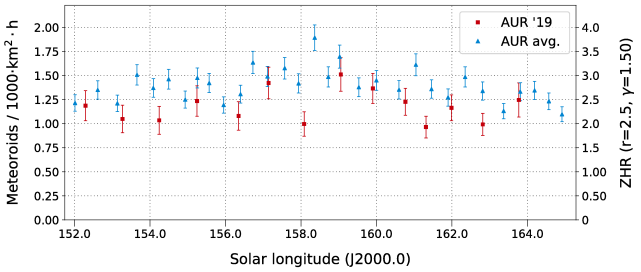

Figure 14 – Flux density of the α-Aurigids in 2019 (red squares) along with in the average of the years 2011–2018 (blue triangles), derived from observations of the IMO Network.

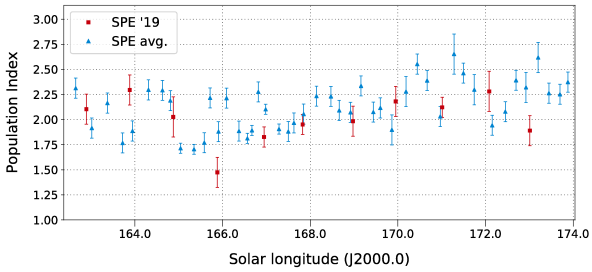

Figure 17 – Population index of the September ε-Perseids in 2019 (red squares) along with the average of the years 2011–2018 (without 2013, blue triangles), derived from observations of the IMO Network.

2014; Gajdoš et al., 2014). According to the IMO Meteor Shower Calendar we did not expect enhanced activity in 2019 (Rendtel, 2018). Only Mikiya Sato predicted possible outbursts at a solar longitude of 166.°801 in 2018 and at a solar longitude of 166.°831 in 2019. A quick look at the activity profile (Figure 15) confirms this prognosis for 2019.

When we increase the temporal resolution (Figure 16) we see a short outburst on 2019 September 10, near $01^{h}10^{m}$ UT (166.°79 solar longitude). The peak solar longitude fits better with the prediction for 2018 than with that for 2019. With about 17 meteoroids per 1 000 km^2 per hour, the activity was not as high as in previous outbursts, but it was still three times the average activity. The full width at half maximum (FWHM) was just half an hour.

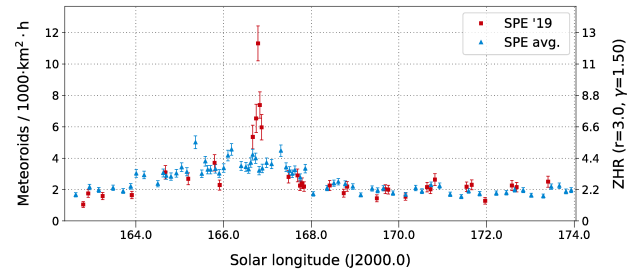

Figure 15 – Flux density of the September ε-Perseids in 2019 (red squares) along with the average of the years 2011–2018 (without 2013, blue triangles), derived from observations of the IMO Network.

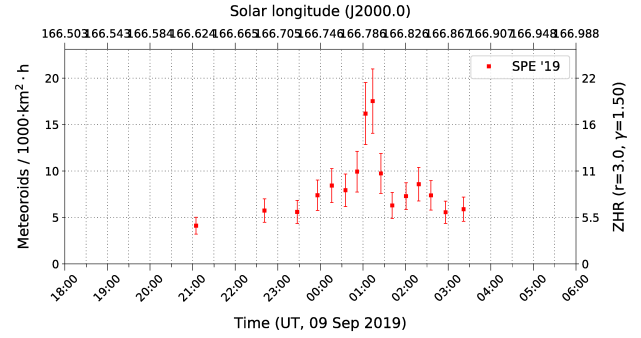

Figure 16 – Flux density of the September ε-Perseids near their peak in 2019, derived from observations of the IMO Network.

The population index was $r = 1.6$ during the peak night. In the other nights, it scattered between $r = 1.75$ and $r = 2.25$ similar to the long-term profile (Figure 17, without 2013).

References

Gajdoš Š., Tóth J., Kornoš L., Koukal J., and Piffl R. (2014). "The September epsilon Perseids in 2013". *WGN, Journal of the IMO*, **42:2**, 48–56.

Jenniskens P., Brower J., Martsching P., Lyytinen E., Entwistle D., and Cooke W. J. (2008). "September Perseid Meteors 2008". *Central Bureau Electronic Telegrams*, **1501**, 1.

Molau S., Kac J., Crivello S., Stomeo E., Barentsen G., and Goncalves R. (2013). "Results of the IMO Video Meteor Network - September 2013". *WGN, Journal of the IMO*, **41:6**, 207–211.

Rendtel J. (2018). "2019 Meteor Shower Calendar". International Meteor Organization. IMO INFO(2-18).

Rendtel J., Lyytinen E., Molau S., and Barentsen G. (2014). "Peculiar activity of the September epsilon-Perseids on 2013 September 9". *WGN, Journal of the IMO*, **42:2**, 40–47.

Rendtel J. and Molau S. (2015). "Enhanced kappa-Cygnid activity 2014". *WGN, Journal of the IMO*, **43:2**, 43–46.

Handling Editor: Javor Kac

Table 1 – Observational statistics for third quarter of 2019.

Code	Name	Place	Camera	July			August			September		
				Nights	Time [h]	Meteors	Nights	Time [h]	Meteors	Nights	Time [h]	Meteors
ARLRA	Arlt	Ludwigsfelde/DE	LUDWIG2	27	89.5	598	26	124.9	932	23	136.2	897
BERER	Berkó	Ludanyhalaszi/HU	HULUD1	8	44.5	191	20	126.5	1008	11	101.8	437
BIATO	Bianchi	Mt. San Lorenzo/IT	OMSL1	24	115.1	427	29	180.0	1098	26	176.9	518
BOMMA	Bombardini	Faenza/IT	MARIO	26	141.0	714	31	206.1	1692	23	188.4	855
BRIBE	Klemt	Herne/DE	HERMINE	25	98.7	417	26	128.1	760	22	128.0	478
		Berg. Gladbach/DE	KLEMOI	26	100.9	426	27	138.1	875	20	134.7	534
CARMA	Carli	Monte Baldo/IT	BMH2	27	148.8	905	31	166.8	1337	27	201.1	1170
CASFL	Castellani	Monte Baldo/IT	BMH1	27	146.8	392	30	147.4	531	24	187.3	426
CINFR	Cineglosso	Faenza/IT	JENNI	25	141.8	612	31	211.5	1823	22	195.8	884
CRIST	Crivello	Valbrevenna/IT	ARCI	30	157.0	742	31	213.6	1453	27	196.4	647
			BILBO	30	154.0	827	30	205.8	1572	27	187.9	793
			C3P8	29	131.1	526	30	167.5	1103	26	170.3	566
			STG38	16	50.6	262	31	207.4	1819	28	215.3	1181
ELTMA	Eltri	Venezia/IT	MET38	29	101.7	395	28	127.2	979	26	104.7	632
FORKE	Förster	Carlsfeld/DE	AKM3	20	76.6	472	26	144.2	1017	20	117.5	532
GONRU	Goncalves	Tomar/PT	TEMPLAR1	28	162.2	708	30	198.2	1184	30	221.1	966
			TEMPLAR2	27	157.8	538	30	199.8	1050	30	226.9	753
			TEMPLAR3	23	130.9	210	28	172.7	469	28	215.4	328
			TEMPLAR4	29	140.0	550	29	189.9	1229	29	222.4	706
			TEMPLAR5	26	136.5	445	29	164.8	1105	29	208.4	751
GOVMI	Govedič	Središče ob Dr./SI	ORION2	26	88.7	275	17	86.6	456	23	71.3	450
			ORION3	12	54.8	87	26	152.2	439	21	116.2	202
			ORION4	11	45.2	82	26	139.7	395	22	113.3	169
HINWO	Hinz	Schwarzenberg/DE	HINWO1	25	99.4	417	29	163.0	968	23	151.9	625
IGAAN	Igaz	Budapest/HU	HUPOL	22	84.0	84	27	167.4	219	17	109.8	87
JONKA	Jonas	Budapest/HU	HUSOR	—	—	—	29	181.7	564	24	165.2	321
			HUSOR2	21	109.5	212	29	181.7	567	21	145.8	299
KACJA	Kac	Kamnik/SI	CVETKA	17	80.5	464	18	105.6	854	15	103.8	662
			REZIKA	17	83.4	480	18	106.7	823	15	122.9	1068
			STEFKA	17	81.5	292	18	109.7	580	15	109.4	433
		Kostanjevec/SI	METKA	6	14.6	60	27	156.2	368	22	145.9	312
		Ljubljana/SI	SRAKA	23	74.2	303	23	93.0	494	19	130.2	449
KNOAN	Knöfel	Berlin/DE	ARMEFA	13	44.0	117	21	115.5	420	22	135.7	272
KOSDE	Koschny	La Palma/ES	ICC7	29	174.8	476	28	181.6	564	21	86.3	226
			ICC9	—	—	—	24	149.8	899	29	204.4	1040
			LIC1	27	153.5	720	28	161.8	961	21	90.5	358
			LIC2	—	—	—	23	188.3	2387	28	254.6	2768
KWIMA	Kwinta	Krakow/PL	PAV06	17	63.6	112	23	129.7	349	16	101.0	156
			PAV07	19	64.1	123	23	128.9	358	16	101.2	153
			PAV79	19	72.8	228	23	136.1	529	16	107.1	314
MACMA	Maciejewski	Chelm/PL	PAV35	9	30.9	126	27	122.5	803	18	107.7	321
			PAV36	9	39.4	212	27	142.4	1249	19	124.3	540
			PAV43	9	36.6	175	27	138.4	977	19	123.3	478
			PAV60	10	34.3	272	27	136.8	1128	16	116.4	621
MARRU	Marques	Lisbon/PT	CAB1	29	181.2	549	31	227.5	1480	30	233.2	714
			RAN1	24	102.5	274	29	182.8	1093	29	203.3	518
MISST	Missiaggia	Nove/IT	TOALDO	21	102.5	684	28	124.5	1136	18	117.9	623
MOLSI	Molau	Seysdorf/DE	AVIS2	27	104.9	841	29	119.1	1055	26	157.4	1119
			DIMCAM2	25	113.7	1338	25	113.6	1603	24	149.5	1610
			ESCIMO3	26	121.7	755	26	124.6	835	23	157.5	902
		Ketzür/DE	REMO1	28	99.8	923	28	138.2	1328	25	144.0	1197
			REMO2	27	98.3	638	28	128.4	859	26	152.9	811
			REMO3	26	110.3	673	29	159.9	1059	24	164.6	849
			REMO4	26	109.7	864	30	158.9	1365	26	172.2	1148
MORJO	Morvai	Fülöpszallas/HU	HUFUL	28	148.2	228	28	190.2	513	26	182.9	308
MOSFA	Moschini	Rovereto/IT	ROVER	24	115.1	197	30	131.5	439	24	156.1	246
NAGHE	Nagy	Budapest/HU	HUKON	29	46.9	365	23	108.5	856	15	85.8	306
		Piszkestetö/HU	HUPIS	31	132.0	531	30	197.8	1193	22	115.3	605
OTTMI	Otte	Pearl City/US	ORIE1	4	19.4	49	24	58.8	132	8	3.3	17
PERZS	Perkó	Becsehely/HU	HUBEC	26	111.2	439	27	160.6	862	20	127.4	537
SARAN	Saraiva	Carnaxide/PT	RO1	30	208.2	491	30	202.7	896	27	241.8	550
			RO2	30	202.1	627	29	208.5	1047	30	250.4	758
			RO3	31	232.5	856	31	244.1	1778	30	258.6	1024
SCALE	Scarpa	Alberoni/IT	LEO	26	113.3	154	22	116.9	364	—	—	—
SCHHA	Schremmer	Niederkrüchten/DE	DORAEMON	25	94.6	354	24	139.4	705	22	129.4	484
SLAST	Slavec	Ljubljana/SI	KAYAK1	15	57.9	183	21	110.6	439	19	115.3	336
			KAYAK2	19	89.8	126	21	115.6	231	22	138.2	158
STOEN	Stomeo	Scorze/IT	MIN38	29	112.8	716	30	143.8	1400	29	180.7	1198
			NOA38	29	135.0	579	30	155.2	1191	28	194.6	844
			SCO38	27	103.9	687	30	147.0	1628	29	182.6	1186
STRJO	Strunk	Herford/DE	BEMCE	—	—	—	11	77.6	853	20	120.3	1191
			MINCAM2	23	92.7	578	28	154.1	1205	25	131.6	676
			MINCAM3	23	76.4	255	27	100.8	688	20	110.0	478
			MINCAM4	20	88.0	157	28	146.1	381	20	118.6	212
			MINCAM5	23	84.9	201	28	139.8	631	19	78.6	241
			MINCAM6	23	83.2	299	16	67.0	600	—	—	—
TEPIS	Tepliczky	Agostyan/HU	HUAGO	18	63.6	178	26	136.2	353	18	137.4	187
			HUMOB	23	85.9	300	29	162.1	1124	23	170.6	823
WEGWA	Wegrzyk	Nieznaszyn/PL	PAV78	12	35.0	128	24	84.4	427	23	86.1	285
YRJIL	Yrjölä	Kuusankoski/FI	FINEXCAM	—	—	—	22	93.5	514	23	127.8	420
ZAKJU	Zakrajšek	Petkovec/SI	PETKA	12	50.0	252	17	98.6	484	25	170.1	919
			TACKA	10	39.5	74	16	82.9	202	22	154.2	350
Sum				31	7722.0	32 217	31	12 047.6	73 336	30	11 994.9	50 208

The International Meteor Organization

www.imo.net

Follow us on Facebook InternationalMeteorOrganization

Follow us on Twitter @IMOMeteors

Council

President: Cis Verbeeck,
Bogaertsheide 5, 2560 Kessel, Belgium.
e-mail: cis.verbeeck@gmail.com

Vice-President: Juraj Tóth,
Fac. Math., Phys. & Inf., Comenius Univ.,
Mlynska dolina, 84248 Bratislava, Slovakia.
e-mail: toth@fmph.uniba.sk

Secretary-General: Robert Lunsford,
14884 Quail Valley Way, El Cajon,
CA 92021-2227, USA. tel. +1 619 755 7791
e-mail: lunro.imo.usa@cox.net

Treasurer: Marc Gyssens, Heerbaan 74,
B-2530 Boechout, Belgium.
e-mail: marc.gyssens@uhasselt.be
BIC: GEBABEBB
IBAN: BE30 0014 7327 5911
Bank transfer costs are always at your expense.

Other Council members:
Karl Antier, 16, rue de la République,
F-04100 Manosque, France.
e-mail: karl.antier@gmx.fr
Javor Kac (see details under WGN)
Detlef Koschny, Zeestraat 46,
NL-2211 XH Noordwijkerhout, Netherlands.
e-mail: detlef.koschny@esa.int
Sirko Molau, Abenstalstraße 13b, D-84072
Seysdorf, Germany. e-mail: sirko@molau.de
Francisco Ocaña Gonzalez, C/ Arquitectura, 7.
28005 Madrid, Spain.
e-mail: francisco.ocana.gonzalez@gmail.com
Vincent Perlerin, 16, rue Georges Bernanos,
51100 Reims, France.
e-mail: vperlerin@gmail.com
Jürgen Rendtel, Eschenweg 16, D-14476
Marquardt, Germany. e-mail: jrendtel@aip.de

Commission Directors

Visual Commission: Jürgen Rendtel
Generic e-mail address: visual@imo.net
Electronic visual report form:
http://www.imo.net/visual/report/electronic
Video Commission: Sirko Molau (video@imo.net)
Photographic Commission: Bill Ward
(bill_meteor@yahoo.com)
Generic e-mail address: photo@imo.net
Radio Commission: Chris Steyaert
(radio@imo.net)
Fireballs: Online fireball reports:
http://fireballs.imo.net

Webmaster

Karl Antier, e-mail: webmaster@imo.net

WGN

Editor-in-chief: Javor Kac
Na Ajdov hrib 24, SI-2310 Slovenska Bistrica,
Slovenia. e-mail: wgn@imo.net;
include METEOR in the e-mail subject line

Editorial board: Ž. Andreić, D.J. Asher,
F. Bettonvil, M. Gyssens, C. Hergenrother,
T. Heywood, J.-L. Rault, J. Rendtel,
C. Verbeeck, S. de Vet, D. Vida.

IMO Sales

Available from the Treasurer or the Electronic Shop on the IMO Website	€	$
IMO membership, including subscription to WGN Vol. 50 (2022)		
Surface mail	26	32
Air Mail (outside Europe only)	49	60
Electronic subscription only	21	25
Proceedings of the International Meteor Conference on paper		
1990, 1991, 1995, 1996, 1999, 2000, 2002, 2003, per year	9	12
2007, 2010, 2011, per year	15	20
2012, 2013, 2015, 2017 per year	25	32
Proceedings of the Meteor Orbit Determination Workshop 2006	15	20
Radio Meteor School Proceedings 2005	15	20
Handbook for Meteor Observers	23	29
Meteor Shower Workbook	12	16
Electronic media		
Meteor Beliefs Project ZIP archive	6	8

Now available!

See page 36 for details

International Meteor Organization

HANDBOOK FOR METEOR OBSERVERS

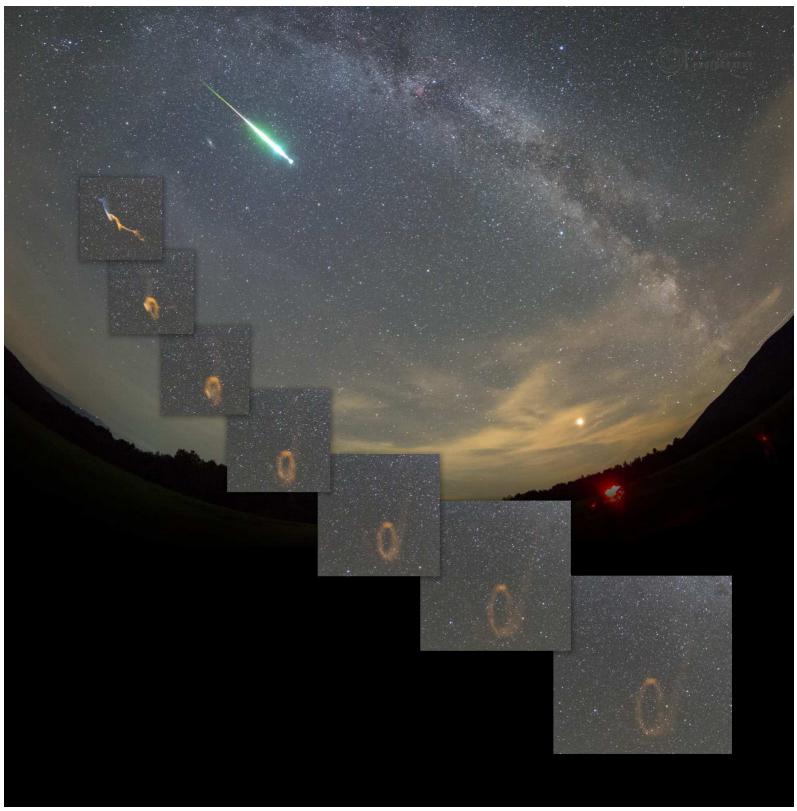

Edited by
Jürgen Rendtel
2022